Triangular tabs for supersonic jet mixing enhancement

Arun Kumar P.
p_arunkumar@cb.amrita.edu
E. Rathakrishnan
erath@iitk.ac.in
Department of Aerospace Engineering
Indian Institute of Technology, Kanpur
Kanpur
India

ABSTRACT

The mixing promoting capability of right-angled triangular tab with sharp and truncated vertex has been investigated by placing two identical tabs at the exit of a Mach 2 axi-symmetric nozzle. The mixing promoting efficiency of these tabs have been quantified in the presence of adverse and marginally favourable pressure gradients at the nozzle exit. It was found that, at all levels of expansion of the present study though the core length reduction caused by both the tabs are appreciable, but the mixing caused by the truncated tab is superior. The mixing promoting efficiency of the truncated tab is found to increase with increase of nozzle pressure ratio (that is, decrease of adverse pressure gradient). For all the nozzle pressure ratios of the present study, the core length reduction caused by the truncated vertex tab is more than that of sharp vertex tab. As high as 84% reduction in core length is achieved with truncated vertex right-angled triangular tabs at moderately overexpanded level, corresponding to expansion level $p_e/p_a = 0{\cdot}90$. The corresponding core length reduction for right-angled triangular tabs with sharp vertex and rectangular tabs are 65% and 31%, respectively. The present results clearly show that the mixing promoting capability of the triangular tab is best than that of rectangular tabs at identical blockage and flow conditions.

Paper 4028. Manuscript received 9 July 2013, revised version received 17 October 2013, third revised version received 7 February 2014, accepted 8 May 2014.

https://doi.org/10.1017/S0001924000009969 Published online by Cambridge University Press

NOMENCLATURE

D_e nozzle exit diameter
L_c core length of the jet
ΔL_c percentage reduction in core length of the controlled jet
M_d design Mach number at the nozzle exit
M_j perfectly expanded Mach number at the nozzle exit
NPR nozzle pressure ratio (p_{0s}/p_a)
p_a atmospheric pressure
p_b backpressure (= p_a)
p_e nozzle exit pressure
p_{0s} settling chamber pressure
p_{0t} Pitot pressure in the jet field
r distance along the radial direction of the uncontrolled jet
Re_j Reynolds number based on the jet velocity and exit diameter
T_0 total temperature in the settling chamber
T_j temperature of the jet at the nozzle exit
U_j perfectly expanded jet velocity at the nozzle exit
w width of the tab
x co-ordinate along the jet axis
y co-ordinate normal to the tabs
z co-ordinate along the tabs
ϕ angle at which the vortex rotates with respect to z-direction
β ratio between inner and outer diameter of the Pitot probe
β_d shock strength parameter
ρ_j density of the jet at the nozzle exit
μ_j dynamic viscosity of the jet at the nozzle exit
χ uncertainty associated with measurements
ϕ_j ratio between the mass flow rate of the microjet and the primary jet

1.0 INTRODUCTION

The mixing process for a jet is a very important determinant of its characteristics. Over the past century, the attempts to improve the effectiveness of jets in their wide variety of applications, have led to numerous technologies aimed at controlling the mixing of the jets. There are numerous systems, especially in aerospace science, where the ability to enhance the mixing characteristics of a jet will greatly improve their performance. For example, by increasing the rate of mixing between the oxidiser and fuel, the efficiency of the combustion cycle can be improved. In scramjet engines, the entire mixing process has to be completed within a short distance to minimise the size of the combustor and for enhancing the performance of the entire vehicle system[1,2]. In combustion systems, both large and small scale mixing enhancement is sought since large scale mixing determines the rapidity of the mixing process and small scale or micro scale level mixing ensures effective molecular level mixing for efficient combustion. By increasing the rate of mixing with the ambient, the infra-red radiance of the plume can be reduced. Other examples of technological applications requiring control of mixing in compressible flows include thrust augmenting ejectors, thrust vector control, metal deposition, and gas dynamic lasers[1,2]. Very broadly speaking, the jet control techniques are used to alter the flow and noise characteristics of jets. The reviews by

https://doi.org/10.1017/S0001924000009969 Published online by Cambridge University Press

Gutmark *et al*[1], Gutmark and Grinstein[2], Seiner *et al*[3] and, Knowles and Saddington[4] provide an extensive survey of mixing enhancement techniques. All types of jet control can be broadly classified into active and passive controls. In active control, an auxiliary power source (microjet [5–8], fluid tabs[9–16] and other techniques[17–23] is used to control the jet characteristics. In passive control the controlling energy is drawn directly from the flow to be controlled. Both active and passive controls mainly aim at modifying the flow and noise characteristics. Among the two main types of jet control, passive controls are mostly desired because no external power source is required. Passive control methods use geometrical modifications which alter the flow structure. Passive control techniques range from alterations in the exit shape of the nozzle (non- circular nozzles[2]) to the, implementation of grooves/notches[24–39], tooth like tabs, swirls[40–46] and chevron nozzles[47–53]. Many studies have focused on the placement of small tabs at the exit of axisymmetric and asymmetric nozzles. These methods primarily aim at disturbing the boundary layer at nozzle exit, which drastically influences the shear layer growth and flow behaviour, thus providing a lot of scope for mixing enhancement.

A tab is essentially a small solid strip kept normal to the flow, usually at the nozzle exit, which generates a pair of counter rotating transverse vortices (with the axis of rotation along the tab), which become streamwise soon after shedding, that can affect the jet flow development significantly. Control of jets using tabs was first documented by Bradbury and Khadem[54]. They studied the effect in a subsonic jet, and observed that the nozzle boundary-layer thickness, turbulence level and convergence had no strong influence on the jet development, compared to the mechanical tabs. Moreover, they came up with an interesting feature that the number of tabs had a direct influence in the jet development. That is, when employing two tabs, the potential core length was drastically, whereas no such significant decrease in potential core length was observed when employing four and eight tabs. Control of a supersonic jet at Mach number 1·12, revealed that the potential core length of the jet could be reduced from about $6D_e$ to less than $2D_e$ by using two mechanical tabs[55,56]. Later on Samimy *et al*,[57,58] studied the effect of small tabs on the characteristics of an axisymmetric jet over the Mach number range of 0·3 − 1·81. They observed a drastic increase in the velocity decay when the tabs were used, reducing the length of the jet potential core. It was found that the tabs distort the jet cross section and increase the jet spread rate significantly[54–61]. The flow field distortion produced by the tabs changes drastically if their location was slightly varied relative to the nozzle exit[62,63]. Visualisation of the jet flow controlled by tabs revealed, that the distortion introduced by a mechanical tab is due to a pair of streamwise vortices and which must be responsible for the phenomenal entrainment [59]. Subsequent researchers have clearly determined that the tab produces a pair of counter-rotating streamwise vortices[60,61,64–67]. There are two possible sources of streamwise vorticity for the flow over a tab[60,61]

(*i*) The pressure hill formed at the tab face, which together with the presence of the wall, produces the pair of counter rotating streamwise vortices and

(*ii*) owing to the pressure gradients on the front and rear surface of the tab, vortices are shed from the sides. Initially, vortices shed by the tab have their axis parallel to the edge; as they proceeds downstream, they get re-oriented by the velocity gradients in the shear layer. Thus, if the tab is tilted downstream, vorticity from primary and secondary sources add together, improving the tab effectiveness.

Bohl and Foss[65] confirmed the creation of an upstream pressure hill which produced two regions of concentrated vorticity into the flow on each side of the tab. Steffen *et al*[68], compared numerical results with corresponding experimental results and noted good agreement in terms of the vorticity field as well as overall jet entrainment. These results lent further credence to the postulations made on the basic flow dynamics that manipulation of the size of the vortices

https://doi.org/10.1017/S0001924000009969 Published online by Cambridge University Press

shed by a tab plays a dominant role in promoting the mixing of free jets[60,61]. The size of the vortices plays a dominant role in both near field and far field mixing of the jet. It is also evident that, for an efficient mixing of the mass entrained by the large scale vortices, at the boundary of a free jet, an appropriate proportion of mixing promoting vortices need to be introduced into the jet flow, to ensure rapid mixing[69]. It is well known that, the vortex shed by an object is proportional to the half-width of the object[70], therefore a tab capable of shedding mixing promoting vortices of continuously varying size might prove to be a better mixing promoter than vortices of uniform size[71].

The effect of introducing a 3D shape to the tab geometry, rather than plain 2D tabs of small thickness revealed that, the mixing improvement for all 3D tabs was substantially reduced compared to the plain 2D tab results for the same projected area[72]. The mixing of the jet was also, found to be a strong funtion of the tab projected area, tab width and number of tabs[73]. It has been found that two tabs distort the jet from axisymmetric state more dramatically than four or eight tabs[54–61,74]. However, the tabs used for improving the spreading of jets will result in thrust loss when placed at the nozzle exit. This feature was extensively studied by Zaman[75,76] and reported that there exists an optimum size of the tab, for which the gain in jet spreading is maximum per unit loss of thrust coefficient. It was shown that for a given nozzle, the base width of the delta tabs can be increased only up to a limit, which is 0·14 (w/D_e) with negligible (5%) thrust loss. Also, the thrust loss varied approximately linearly with the geometric blockage; that is, thrust loss / (w/D_e) = constant, for $w/D_e \leq 0{\cdot}28$. However, with further increase in the tab size the variation is no longer linear[75,76].

It is evident from the preceding discussion that, the size of the vortices play a dominant role in both the near field and far field of the jet mixing and also the vortex shed by an object is proportional to the half-width of the object. Therefore a tab capable of shedding mixing promoting vortices of continuously varying size might prove to be a better mixing promoter than vortices of uniform size. With this aim, in the present study right-angled triangular tabs have been used for promoting the mixing of a Mach 2 axi-symmetric free jet, in the presence of adverse pressure gradients and marginally favourable pressure gradient. The mixing promoting efficiency of two right-angled triangular tabs, located at diametrically opposite ends, at the exit of a Mach 2 convergent-divergent circular nozzle has been studied. In addition to the right-angled triangular tabs, offering an area blockage of 5% (2·5% each), rectangular tabs of the same blockage were also studied for comparison. One more aspect considered in this investigation is the tip geometry of the triangular tab. If the tip is sharp, the vortices near the tip might counteract each other, thereby they might lose a part of the mixing promoting capability. To understand this aspect, two right-angled triangular tabs with truncated vertex were also studied. It is well established that, the centreline Pitot pressure decay can be taken as a direct measure of jet mixing. Therefore, to study the mixing promoting capability of the triangular and rectangular tabs, the centreline Pitot pressure decay for the uncontrolled and controlled jets were measured at NPRs 4, 5, 6, 7 and 8 giving the expansion ratio (p_e/p_a) at the nozzle exit of 0·511, 0·639, 0·767, 0·895, 1·022, respectively, for the Mach 2 nozzle. The flow downstream of the nozzle exit is determined by these pressure ratio. Such that, the expansion ratio with 0·511 and 0·639 are termed as highly overexpanded state, expansion ratio with 0·767 and 0·895 are termed as moderately overexpanded state and expansion ratio with 1·022 is called as marginally underexpanded state. In addition to the centreline decay, the Pitot pressure distribution in the planes normal to the jet axis, at different axial locations (x/D_e), were also measured. The waves prevailing in the uncontrolled and controlled jets have been visualised by shadowgraph method.

https://doi.org/10.1017/S0001924000009969 Published online by Cambridge University Press

2.0 EXPERIMENTAL FACILITY AND PROCEDURE

The experiments for the present study were conducted in the High Speed Aerodynamics Laboratory at the Indian Institute of Technology Kanpur. The test facility consists of air supply system (compressors and storage tanks) and open jet testing facility.

2.1 Air supply system

A two-stage reciprocating compressor, capable of delivering 0·17m^3/sec of air at a pressure of 3·5MPa is used in the air supply system. The compressor is driven by a 112kW three-phase induction motor. A cooling water circuit, driven by an independent pump, cools the compressed air through an inter-cooler. The compressed air is then passed through a pre-filter consisting of porous stone candles to remove solid contaminants like rust particles and oil droplets. An activated carbon filter is used for finer filtering of the air. The compressed air is dried in a dual-tower semi-automatic silica gel dryer. While one tower is in use, a portion of the dried air is heated and used to reactivate the other. A diaphragm type backpressure valve operated by pressure relief pilot permits the dryer to operate at 3·5MPa, while the pressure in the storage tanks builds up from atmospheric to the required storage pressure. The compressed air is stored in three tanks, having a total capacity of 85m^3.

2.2 Open jet facility

The open jet facility consists of a cylindrical settling chamber connected to high pressure storage tanks. A schematic diagram of the open jet facility is given in Fig. 1. The compressed air to the settling chamber was supplied from the storage tank through a control valve. To reduce the flow disturbance caused by the control valve, a mixing length of 1m was placed between the valve and the settling chamber. The settling chamber is connected to the mixing tube by a wide angle diffuser. The settling chamber has a constant area circular section of 300mm inside diameter and 600mm length. The flow was conditioned, by two wire mesh screens placed in the settling chamber, before entering into the nozzle. The settling chamber has tapings for stagnation pressure and temperature measurements. The test models were fixed at the end of the settling chamber by a slot holder arrangement, which is a short pipe like protrusion with an embedded O-ring to prevent leakage. The convergent-divergent nozzle of the present investigation was placed over the O-ring, over which an annular retaining sleeve with internal threads is screwed tightly. The settling chamber total pressure (p_{0s}) was maintained constant during a run, by manually controlling the pressure regulating valve. The settling chamber temperature (T_{0s}) was the same as the ambient temperature (T_a) and the backpressure (p_b) was the pressure of ambient (p_a) to which the jets were discharged.

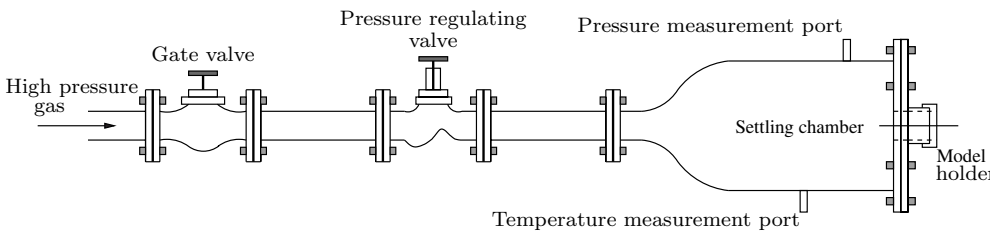

Figure 1. Schematic layout of the open jet facility.

https://doi.org/10.1017/S0001924000009969 Published online by Cambridge University Press

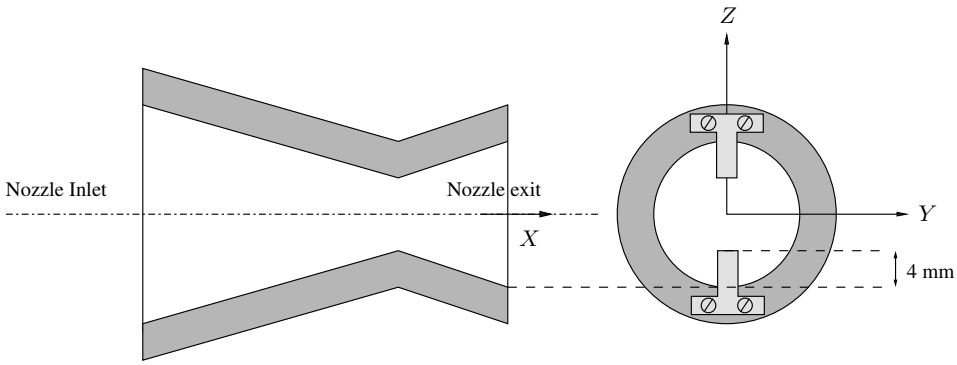

Figure 2. Schematic representation of nozzle and placement of tabs at the nozzle exit (D^* = 10·02mm, D_e = 13·02mm, A_e/A^* = 1·688, M_d = 2·0, Design *NPR* = 7·824, Lip thickness = 5mm; The uncertainty in measurement was ±0·02mm).

2.3 Experimental model

The experimental model used in the present investigation is a Mach 2·0 axisymmetric convergent-divergent nozzle of semi-divergence angle 7°, made of brass. The throat diameter (D^*) of the nozzle is 10·02mm and an expansion section of 12·22mm in axial length. The exit diameter (D_e) is 13·02mm, giving the nozzles area ratio of 1·688. This area ratio corresponds to a design exit Mach number of 2·0 and the corresponding design nozzle pressure ratio (NPR) is 7·824. The Reynolds numbers of the jet coming out of the nozzle, are $0{\cdot}72 \times 10^6$ and $1{\cdot}2 \times 10^6$ respectively, for the minimum and maximum NPRs of 4 and 8 of the present investigation. The Reynolds number, Re_d, is based on ρ_j , U_j , D_e and u_j where U_j is the jet velocity, ρ_j is determined using isentropic relation and μ_j is calculated based on Sutherland's formula.

The tabs for the investigation was made of 1mm brass strips. The length of the tabs was kept constant at 4mm for both right-angled triangular and rectangular shapes. This was done to ensure that all the tabs sheds vortices upto the same distance along the radial direction of the nozzle. The

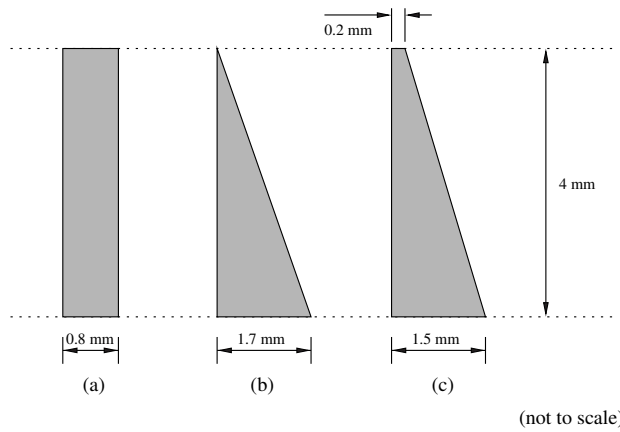

Figure 3. Schematic representation of different tab geometries (a) rectangular tab, (b) right-angled triangular with sharp vertex tab and (c) right-angled triangular with truncated vertex tab; The uncertainty in measurement was ±0·02mm.

https://doi.org/10.1017/S0001924000009969 Published online by Cambridge University Press

Table 1
Test conditions

M_d	*NPR*	M_j	T_0 (K)	U_j (ms^{-1})	D_e(mm)	Re_j (*10^6)	p_e/p_a	β_d
2·0	4	1·56	303	446·6	13·02	0·72	0·511	–1·25
2·0	5	1·71	303	473·7	13·02	0·79	0·639	–1·04
2·0	6	1·83	303	494·8	13·02	1·0	0·767	–0·81
2·0	7	1·93	303	510·3	13·02	1·1	0·895	–0·52
2·0	8	2·01	303	520·7	13·02	1·2	1·022	+0·20
1·5[53]	**4**	**1·56**	**300**	**444·0**	**74·01**	**3·9**	**1·089**	**+0·42**

manufacturing tolerance on the tab was about ±0·02mm. The schematic representation of nozzle and the tab geometries studies are shown in Figs 2 and 3, respectively. The blockage offered by the two identical tabs, intruding the flow, with respect to the nozzle exit area, of the present investigation is 5%. It is usual practice to keep in jet studies to keep the tab blockage of about 5%, such that the thrust losses are very small[61,75,76].

2.4 Experimental test conditions

The experiments were conducted for the nozzle pressure ratio (NPR), which is defined as the ratio of stagnation pressure (p_{0s}) to the backpressure ($p_b = p_a$) of the nozzle from 4 to 8. The corresponding equivalent (perfectly expanded) Mach number (M_j), is in the range from 1·56 to 2·01. The equivalent (perfectly expanded) Mach number (M_j) is defined as the Mach number which will be obtained from isentropic relations corresponding to that *NPR*.

The nozzle pressure ratios used, the corresponding fully expanded jet Mach numbers, M_j, and other parameters of interest are shown in Table 1. β_d is a shock strength parameter defined $\beta_d = \pm\sqrt{(|M_e^2 - M_j^2|)}$ where the plus sign is taken for underexpanded cases when M_j is greater than M_e , and the minus sign is taken for overexpanded cases when M_j is less than M_e. This parameter reduces to the β_d introduced by Harper-Bourne and Fischer[77] for convergent nozzles where $M_e = 1{\cdot}0$.

Calibration of the nozzle is important, since there is a possibility of actual Mach number to differ from the design Mach number. Therefore, the Pitot probe was moved from one end of the nozzle exit to the other end. The nozzle was operated at several values of p_{0s} , such that the nozzle is chocked and which is well above the shock-free condition in the nozzle[78], and multiple readings of p_{0t} were taken for each case. In the case of a supersonic free-stream, a probe will cause the formation of a detached shock, hence a Pitot pressure probe will measure only the total pressure (p_{0t}) behind the bow shock at the nose. Because of the non-isentropic nature of the compression through the shock wave, the Bernoulli equation cannot be used. Treating the flow through the nozzle to be isentropic (shock-free), such that total pressure in the settling chamber to be equal to the total pressure at the nozzle exit. Furthermore, treating the portion of detached shock to be a normal shock at the axis of the pitot probe. The measured Pitot pressure (p_{0t}) can be used to determine the Mach number from the settling chamber pressure (p_{0s}),thus the Mach number in-terms of p_{0t} and p_{0s}[79, 80]

$$\frac{p_{0t}}{p_{0s}} = \left(1 + \frac{2\gamma}{\gamma+1}(M_d^2 - 1)\right)^{\frac{-1}{\gamma-1}} \left(\frac{(\gamma+1)M_d^2}{(\gamma-1)M_d^2 + 2}\right)^{\frac{\gamma}{\gamma-1}} \quad \ldots (1)$$

can be used to obtain M_d from the measured values of p_{0t}. The average of all such values of M_d was found to be 2·0.

https://doi.org/10.1017/S0001924000009969 Published online by Cambridge University Press

2.5 Instrumentation

In the present investigation the pressure sensing probe used was the conventional Pitot probe. The Pitot tube has 0·4mm inner diameter and 0·6mm outer diameter. The Pitot probe was mounted on a three-dimensional traverse. The traverse has six degrees of freedom, which also includes a probe-yawing mechanism. The traverse has a linear resolution of 0·1mm in all the three directions, i.e. the positioning accuracy of the probe was within ±0·1mm in all the three directions.

The accuracy of the probe depends on its nose shape, the Reynolds number, the magnitude of transverse shear, turbulence intensity, turbulence length scale, the orientation with respect to the mean flow direction and the Mach number[81]. The pressures measured by Pitot probe could be significantly influenced by low Reynolds numbers based on the probe diameter. However, this effect will not cause any error when the Reynolds number of the pitot probe is above 500[79–81]. FFor the present probe of outer diameter 0·6mm, the Reynolds number at NPRs 4 and 8 are $3{\cdot}3 \times 10^4$ and $5{\cdot}5 \times 10^4$, respectively. Hence the viscous effect will not cause any error in the Pitot pressure measurements.

A pitot probe may experience an incoming flow that is not parallel to its centreline due to physical misalignment to the predominant flow direction (which may be eliminated by careful experimental setup). The directional sensitivity of the probe will depend on the tip shape, probe diameter ratio (ϕ = inner diameter / outer diameter), and the Mach and Reynolds numbers[80,81]. For the present square-ended pitot probe, with $\phi = 0{\cdot}67$, the yaw sensitivity is about ±11°[80, 81]. Moreover, the yaw sensitivity decreases with increase in Mach number of the incoming flow[81].

The Pitot pressure measured in the supersonic regime is the total pressure behind the bow shock that stands ahead of the probe. Thus, it is not the actual total pressure. If the actual total pressure is required one has to correct for the pressure loss across the shock. Since the supersonic jet core is wave dominated, the Mach number in the core varies from point to point and also the shocks in different cells are of varying strength. Therefore, no attempt is made to correct the measured total pressure for shock loss. It has to be emphasised that in supersonic regions there is some measurement error due to probe interference with shock structure and so the measured pressure data in supersonic regions should be considered only qualitative and good enough for comparative study. However, the difference between the measured results from a Pitot tube and the actual ones is about 5%[82,83]. The pressure oscillations in the core region of the supersonic flow are due to the shock cells in the jet. Nevertheless, the data is accurate enough to capture the overall features, such as the supersonic core length, number of shock cells and the shock-cell length. In a supersonic flow maxima in Pitot pressure correspond to minima in Mach number and vice versa[69].

2.6 Pressure transducer and application software

Pressures were measured with a 16 channel Pressure Systems, Inc 9010 transducer with a range of 0–2·1MPa. The software provided by the manufacturer was used to interface the transducer with a computer. The user-friendly menu-driven software acquires data and shows the pressure reading from all 16 channels simultaneously in a window-type display on the computer screen. The software can be used to choose the units of pressure from a list of available units, perform a rezero/full calibration, etc. The transducer also has a facility to choose the number of samples to be averaged by means of dip-switch settings. The accuracy of the transducer (after rezero calibration) is specified to be ±0·15% full scale.

However, it is important to note that the jet pressure field is essentially unsteady due to the vortices prevailing in the flow field. Therefore, what is measured is the mean value of the Pitot

https://doi.org/10.1017/S0001924000009969 Published online by Cambridge University Press

pressure. To make this measurement with acceptable accuracy, the provision available in the transducer, namely the average of 250 samples per second, for a time duration of 60 seconds has been exploited to record the Pitot pressure. That is, every Pitot pressure measured is the average value of 15,000 samples.

2.7 Shadowgraph technique

The shadowgraph technique is suitable for visualising the flow field where strong gradients exist. Supersonic and underexpanded sonic jet flows produce large density gradients that lead to variations in optical refractive index of the light that passes through the supersonic flow. The light beam is refracted wherever there is a density gradient in the flow field. However, if the density gradient everywhere in the flow field is constant, all light rays deflect by the same amount, and there is no change in the illumination of the picture on the screen. Only when there is a gradient in the density gradient, there is a tendency for light rays to converge or diverge. In other words, the variations in illumination of the shadowgraph picture on the screen are proportional to the second derivative of the density.

The waves prevailing in the supersonic jet core were visualised using a shadowgraph system with a helium spark arc light source in conjunction with a concave mirror of 150mm diameter. The light source was collimated by the condenser lens and was then brought to the concave mirror. The parallel beam from the mirror was made to pass through the jet flow field and projected on the screen. The surface finish of the mirror is $\lambda/6$ and the focal length is 1·6m.

2.8 Uncertainty

Error in a scientific measurement means the inevitable uncertainty that is present in all measurements. Errors cannot be eliminated, however the best we can do is to minimise the errors and reliable estimate how large they are[84]. Error signifies the deviation from the true value. However, on repeating the experiments, the results may differ from the previous attempt. So any results had to be given with an uncertainty[85]. Uncertainty analysis is the prediction of the uncertainty interval which will be associated with an experimental results[86–88]. Uncertainty should be accounted for, if any measurements was done with the use of instruments. That is, the instrument itself will have some inaccuracy.

In the present work, the ambient pressure (p_a) was measured by a mercury barometer which has a resolution of ±0·1mm, thereby the uncertainty associated in the measurement of atmospheric pressure was 97,927 ± 14Pa, which is about ±0·014%. The movement of the Pitot probe mounted on the traverse had a resolution of ±0·1mm in the linear translation. The pressure regulating valve was operated manually, therefore there were fluctuations in the measured values of p_{0s}. So the inaccuracies in the measured Pitot pressure should be accounted along with its repeatability of experiments, standard deviation of the mean Pitot pressure values, accuracy of the transducer, uncertainty in atmospheric pressure; all these contributes to the overall uncertainty in Pitot pressure, which was about ±1%. Uncertainty associated with design Mach number (M_d), p_{0f}/p_{0s} and the expansion level (p_e/p_a) are around ±0·01, ±0·02 and ±0·007, respectively. The uncertainty associated with the NPR, Mach number, core length (χL_c) and percentage reduction in core length was within ±1%, ±1%, ±1% and ±2%, respectively. The calculation of uncertainties on a parameters and its propagation into other parameters are done using the method given by John Taylor[84]. The detailed procedure for the calculation of these uncertainties are available in Ref. 89.

https://doi.org/10.1017/S0001924000009969 Published online by Cambridge University Press

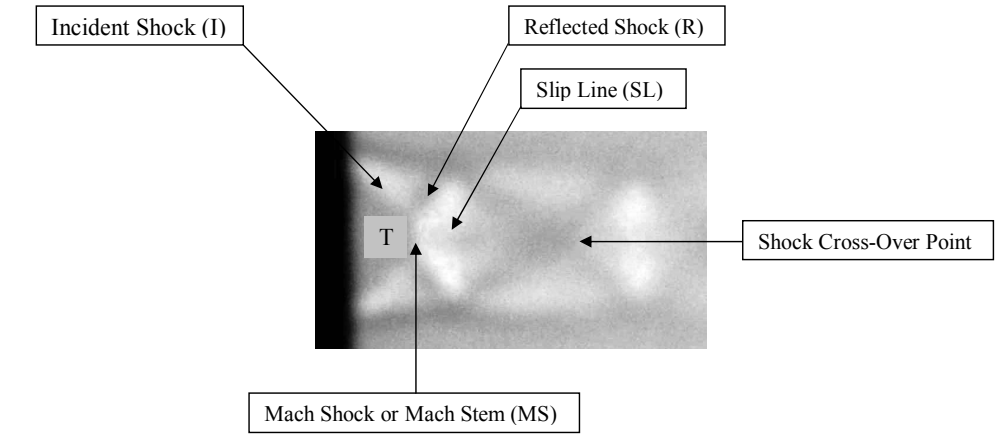

(a) p_e / p_a = 0·511

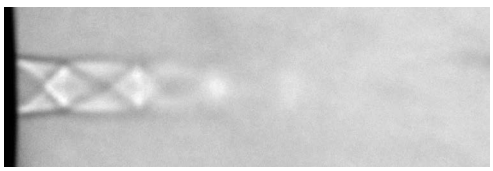

(b) p_e / p_a = 0·639

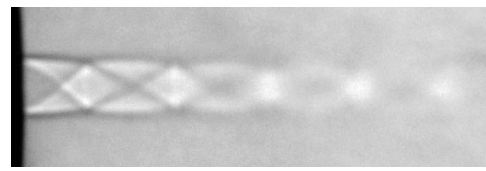

(c) p_e / p_a = 0·767

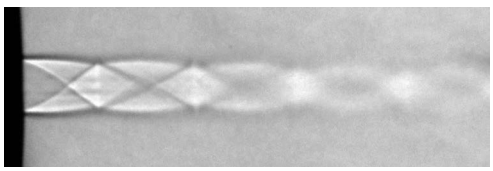

(d) p_e / p_a = 0·895

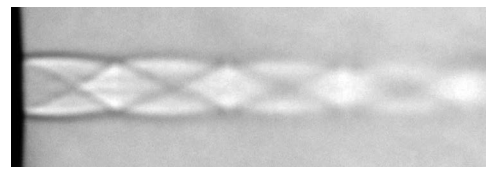

(e) p_e / p_a = 1·022

Figure 4. Shadowgraph pictures for the uncontrolled jet; viewed in the *xy* - plane.

3.0 RESULTS AND DISCUSSIONS

3.1 Flow structure

A converging-diverging nozzle is a device by which uniform supersonic flows can be produced and it will deliver supersonic flow only when the nozzle pressure ratio (p_{0s} / p_a) is greater than the critical value of about 1·89[78]. The shock-cell development in a supersonic jet depends on the nozzle pressure ratio (NPR) and the backpressure (ambient pressure p_a) is the key parameter in determining the nature of the flow in the nozzle and the jet emanating from it. When the exit flow is supersonic, the exit pressure p_e , may be larger, equal, or smaller than p_a. To analyse the development of shock structure in a supersonic jet, qualitative analysis by visualisation technique using shadowgraph method and quantitative analysis using Pitot pressure measurement along the jet centreline had been done for expansion level of 0·511, 0·639, 0·767, 0·895 and 1·022, covering highly overexpanded, moderately overexpanded and marginally underexpanded states.

https://doi.org/10.1017/S0001924000009969 Published online by Cambridge University Press

When $p_e < p_a$, which is an overexpanded state, two oblique shock waves are formed at the lips of the nozzle. The interaction of these oblique shock waves along the jet axis, results in either a regular reflection or a Mach reflection, depending on the level of static pressure ratio (p_e/p_a) at the nozzle exit[90–94]. For an highly overexpanded nozzle free jet flow as in the present case with p_e/p_a = 0·511, the interaction of these oblique shock waves along the jet axis will be of Mach reflection. This is because, since $p_e \ll p_a$, inorder to compress the flow leaving the nozzle exit with static pressure (p_e) to come in equilibrium with the back pressure (p_a), shock with strong in nature called as Mach reflection is formed. The occurrence of such a Mach reflection pattern is always manifested by the appearance of a triple point *T*, somewhere along the straight incident shock wave *I*, where a reflected shock *R*, the Mach shock (or Mach stem) *MS*, and a slipline *SL* (Fig. 4(a)), indicating the entropy discontinuity, are also originated[92,93]. In-order to increase the nozzle exit pressure (p_e), thereby to attain an equilibrium with the backpressure (p_a), Mach shock waves (strong shock) are formed along the centreline, which is almost like a Mach disk (Fig. 4(a)), the flow downstream of this Mach shock (x/D_e = 0·4, Fig. 5(a)) becomes a subsonic. Inspite of considerable transverse exchange of momentum from the higher momentum zone around the subsonic flow behind the Mach disk, the flow accelerates to more than 1·01D_e, only as subsonic flow, and then exhibits a supersonic acceleration upto 1·57D_e. The oblique shock (*R*) are reflected as Prandtl Meyer expansion fans from the jet boundary and further cross each other at the jet centreline. These Prandtl-Meyer expansion fans are further reflected as shock waves from the jet boundary and cross each other at the jet axis named as shock cross-over point, which is about 1·57D_e (Fig. 5(a)). The distance between the Mach shock and the shock cross-over point is called as shock-cell length. After the cross-over point, even though the flow accelerates, possess almost constant Pitot pressure over about 2·34D_e, before becoming supersonic and then exhibits a supersonic acceleration upto 2·74D_e (Fig. 5(a)). This cycle of reflection of shock and Prandtl-Meyer expansion fan continues till the flow finally reaches subsonic thereafter. This process continues upto the end of the supersonic core (L_c), which is found to be around 6·6D_e, for the uncontrolled jet.

An important property that is commonly used to characterise supersonic jets is the supersonic core length (L_c). The supersonic core length is defined as the distance from the nozzle exit to the axial location along the centreline, where the local flow Mach number drops below 1·0. The supersonic core length can be estimated from centreline Pitot pressure surveys[95]. From the centreline Pitot pressure data, the calculation of the supersonic core length was done[71,95].

The pressure measured by the Pitot tube at sonic condition:

$$\frac{p_{0t}}{p_a} = 1{\cdot}893 \qquad \ldots (2)$$

At NPR 4 which corresponds to p_e/p_a = 0·511:

$$\frac{p_{0s}}{p_a} = 4 \qquad \ldots (3)$$

$$\frac{p_{0t}}{p_{0s}} = 0{\cdot}473 \qquad \ldots (4)$$

Similarly the value of p_{0t}/p_{0s}, for other expansion levels can be calculated and is tabulated in

https://doi.org/10.1017/S0001924000009969 Published online by Cambridge University Press

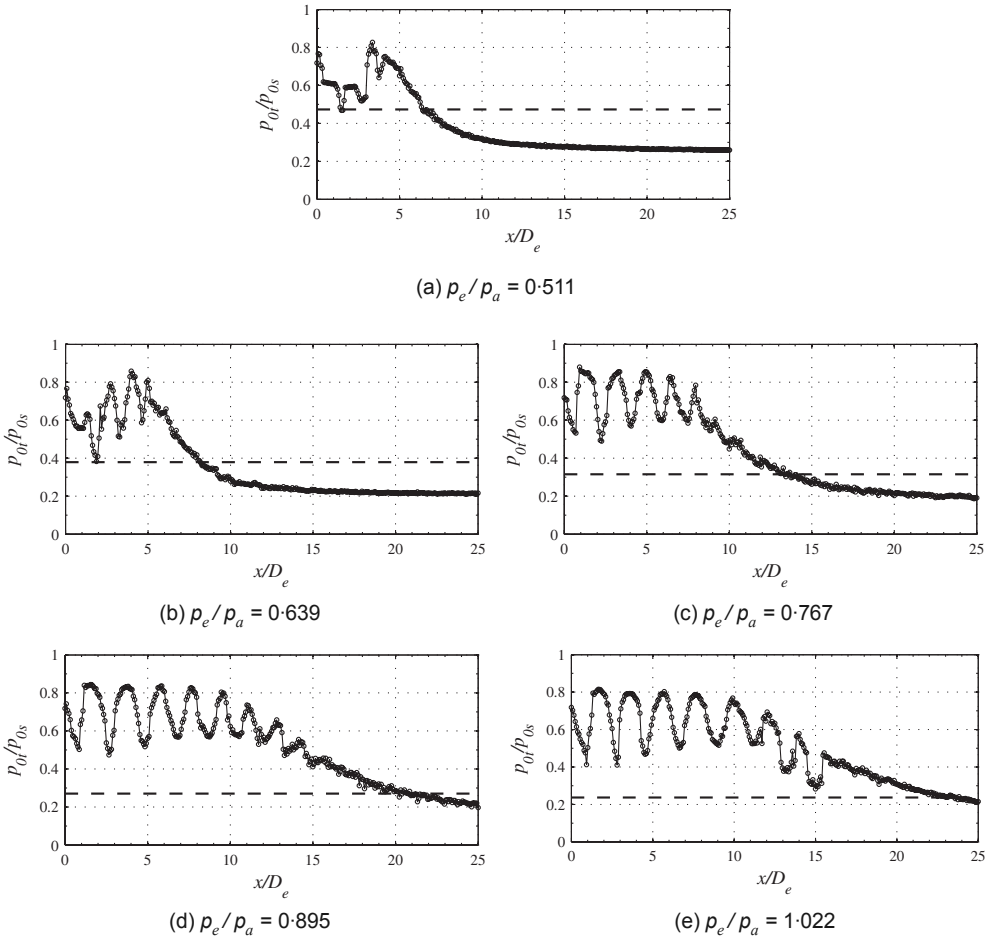

Figure 5. Pitot pressure measurement for the uncontrolled jet; The dotted line shows the cut-off pressure ratio for the supersonic core length as given in Table 2.

Table 2. The axial location along the jet centreline, where the occurrence of p_{0t}/p_{0s}, for a given expansion level gives the extend of supersonic core length. Experimental evidence indicates that the end of the supersonic core, except for near-sonic jets with nearly ambient exit pressure, lies in the region of fully developed, similar flow[96–98]. The dotted line in Figs 5, 8 and 9, denotes the cut-off pressure ratio for the supersonic core length.

With further increase in static pressure at the nozzle exit, that is with p_e/p_a = 0·639, the strength of Mach reflection has decreased as seen from the reduced Pitot pressure at x/D_e = 0·78, in Fig. 5(b). Similar compression effects at the nozzle exit that exhibited at p_e/p_a = 0·511, would prevail at p_e/p_a = 0·639 also, however the strength of the compression wave will depend on the overexpansion level. The dotted line in Fig. 5, denotes the cut-off pressure ratio for the supersonic core length. This line cuts the pitot pressure at x/D_e = 1·57 in Fig. 5(a) and x/D_e = 2 in Fig. 5(b), which are the axial locations of the second cross-over point for p_e/p_a = 0·511 and 0·639, respectively

With further increase in in static pressure at the nozzle exit (p_e/p_a = 0·767), which is at a reduced overexpansion level than at p_e/p_a = 0·511 and 0·639. That is the nozzle exit pressure (p_e) is 0·76 times

https://doi.org/10.1017/S0001924000009969 Published online by Cambridge University Press

Table 2
Pressure ratio for determining the supersonic core length

p_e/p_a	0·511	0·639	0·767	0·895	1·022
p_{0t}/p_{0s}	0·473	0·379	0·315	0·271	0·236

the backpressure (p_a), to which it is discharging. Therefore, in order to compress the flow (exiting the nozzle), to increase the exit pressure (p_e), to come to an equilibrium with the backpressure (p_a), oblique shock waves will be formed at the nozzle exit. At this expansion level, the formation of Mach shock is eliminated because of the increase in static pressure at the nozzle exit, which causes the oblique shock emerged from the nozzle exit to cross each other at a point called as shock cross-over point (seen in Fig. 4(c)). An important feature to be noticed is that, in the present investigation, only one cross-over point was observed, however, two cross-over point was seen by Munday *et al*[99]. The reason being that, first cross-over point is due of the shocks that are formed because of the pressure ratio at the nozzle exit and the second cross-over point is due to the reflection of shock formed because of the sharp throat regardless of the condition outside the nozzle. These shocks of opposite family on either side of the nozzle axis cross each other at the jet axis and travel to the jet boundary and are reflected as expansion waves. In other words, the oblique shocks at the nozzle exit compress the jet flow at a lower pressure pe , come to equilibrium with the ambient pressure pa . It is seen from Fig. 5(c), that the Pitot pressure decreases upto $x/D_e = 0{\cdot}7$, from the nozzle exit. This implies that the supersonic flow accelerates. Because the Pitot pressure measures essentially the total pressure behind the detached shock at the nose of the Pitot probe, it is bound to decrease with increase of supersonic Mach number. After accelerating monotonically up to some axial distance ($x/D_e = 0{\cdot}7$), the pressure ratio assumes the first minimum. This is the point of a local maximum for the Mach number. This can be taken as the location just upstream of the point where the oblique shocks from the opposite ends meet on the jet axis. Just downstream of this shock intersection point, the flow along the jet axis is traversed by two oblique shocks. Even though the individual oblique shocks are weak in nature, their combined strength proves to be strong, causing the flow to become subsonic just behind the intersection point. The subsonic flow downstream of the shock cross-over point receives momentum from the higher momentum flow zones around it. Because of this momentum exchange the subsonic flow accelerates. The region of increasing Pitot pressure from the first pressure minimum point ($x/D_e = 0{\cdot}7$) is the zone of subsonic acceleration, because in a subsonic flow the increase of Pitot pressure is an indication of flow acceleration. The subsonic flow accelerates and attains a sonic state at the point of first peak ($x/D_e = 1{\cdot}1$) in the pressure plot. The sonic flow continues to accelerate to supersonic levels, as indicated by the progressive decrease of Pitot pressure from the first peak point. The supersonic flow attains the second local maximum at the second minimum point ($x/D_e = 2{\cdot}2$) on the pressure plot, which is just ahead of the second cross-over point of the compression waves from opposite ends. Behind this point the flow becomes subsonic and begins to accelerate to sonic level and further accelerates to supersonic levels. This process continues upto the end of the supersonic core, which is found to be around $14{\cdot}1D_e$ (Fig. 5(c)). As the nozzle pressure ratio is further increased, the supersonic core length also increases, as seen in Figs 4 and 5.

3.2 Jet mixing enhancement

The aim of the present investigation is to quantify the mixing promoting efficiency of right-angled triangular tabs with sharp and truncated vertex. To quantify this feature, shadowgraph visualisation and the Pitot pressure measurement in all the three axis of the jet has been done.

https://doi.org/10.1017/S0001924000009969 Published online by Cambridge University Press

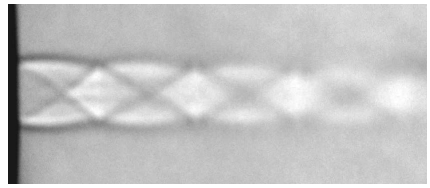

(a) Uncontrolled jet; viewed in the *xy* - plane

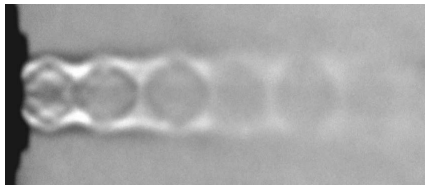

(b) Jet controlled with rectangular tabs; viewed along the tabs (*xy* - plane)

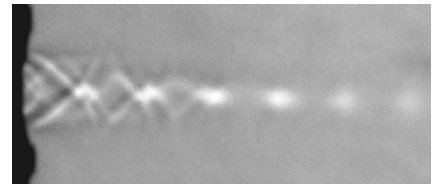

(c) Jet controlled with rectangular tabs; viewed nor- mal the tabs (*xz* - plane)

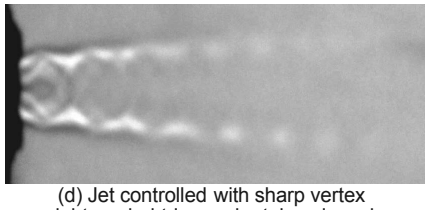

(d) Jet controlled with sharp vertex right-angled tri- angular tabs; viewed along the tabs (xy - plane)

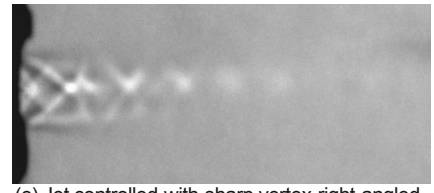

(e) Jet controlled with sharp vertex right-angled tri- angular tabs; viewed normal the tabs (*xz* - plane)

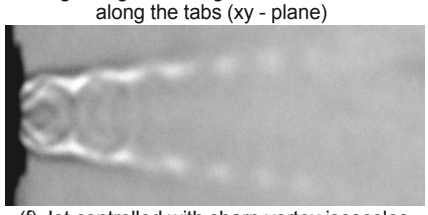

(f) Jet controlled with sharp vertex isosceles triangular tabs; viewed along the tabs (*xy* - plane)

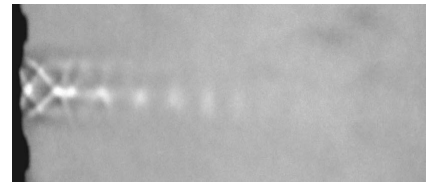

(g) Jet controlled with sharp vertex isosceles triangular tabs; viewed normal the tabs (*xz* - plane)

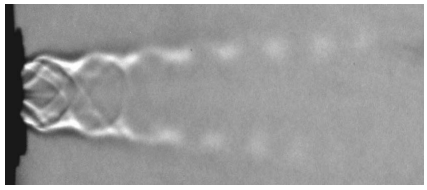

(h) Jet controlled with truncated vertex right-angled triangular tabs; viewed along the tabs (xy - plane)

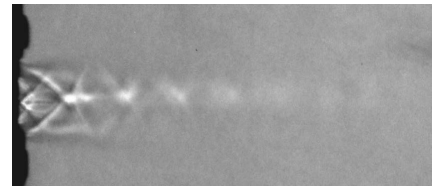

(i) Jet controlled with truncated vertex right-angled triangular tabs; viewed normal the tabs (xz - plane)

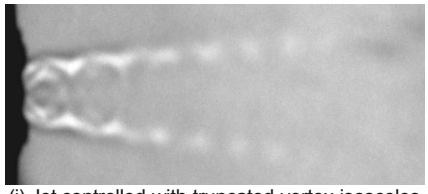

(j) Jet controlled with truncated vertex isosceles tri- angular tabs; viewed along the tabs (xy - plane)

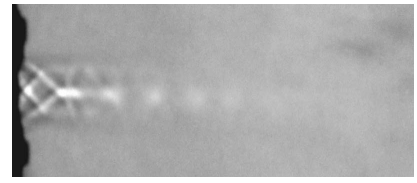

(k) Jet controlled with truncated vertex isosceles tri- angular tabs; viewed normal the tabs (xz - plane)

Figure 6. Shadowgraph pictures for the controlled jets at marginally underexpanded state with p_e/p_a = 1·022.

https://doi.org/10.1017/S0001924000009969 Published online by Cambridge University Press

3.2.1 Optical flow visualisation

The waves prevailing in the core of the uncontrolled and controlled jets was visualised using shadowgraph technique. For the uncontrolled jet, visualisation was done only in the *xy*-plane assuming acceptable degree of accuracy in the other planes, whereas for the jet controlled by tabs, visualisation was done in the planes along (*xy*) and normal (*xz*) to the tabs. A representative set of pictures for the marginally underexpanded state with p_e/p_a of 1·022, are shown in Fig. 6. An important feature to be noted is that in the present investigation, triangular tabs of right-angled geometry was studied. Recent study in modifying the geometry of the triangular tabs, isosceles triangular tabs (Fig. 7) of identical conditions (geometry and flow parameters) was studied by Arun Kumar and Rathakrishnan[71].

The shadowgraph pictures for the isosceles triangular tabs with sharp and truncated vertex are also shown in Fig. 6. For the uncontrolled jet, cycles of shock-cell are seen as explained in Section 3·1. The main observations from these pictures for the jet controlled by tabs, are the absence of the oblique shock wave at the nozzle exit and its associate structures. That is, when the tabs are introduced at the nozzle exit, waves of complex structure are formed in the region very close to the nozzle exit. It is also seen that the shock cells prevailing in the uncontrolled jet are greatly disturbed resulting in a number of smaller diamond like structures. This kind of number of wave crossings is seen up to some downstream distance for all the tabs. Moreover, bifurcation (distortion) of the jet caused by the tabs are also seen for the controlled jets in the *xy*-plane. It is also seen that, in the presence of the tabs, the spread in the *xy*-plane is much larger than the *xz*-plane. Also, the waves in the core for the uncontrolled jet (Fig. 6(a)), are much stronger than the waves prevailing for the controlled jets. For the jet controlled with rectangular tabs (Figs 6(b) and 6(c)), the waves prevailing in the jet core are much stronger than the waves prevailing for the jet controlled with triangular tabs. However, there was no difference seen in the shadowgraph pictures for the jet controlled with right-angled and isosceles triangular tabs.

3.2.2 Centreline pitot pressure decay

It is well established that the centreline Pitot pressure decay is an authentic measure to quantify the jet core length, characteristic decay and far-field decay of free jet[58,60,61,69]. The centreline pressure decay can clearly show the extent of jet core, which is defined as the axial extent up to which the nozzle exit velocity prevails for subsonic jets and the axial extent up to which supersonic flow prevails for supersonic jets. In other words, it can be stated that the core of a jet, either subsonic or supersonic is the distance from nozzle exit at which the characteristic decay begins. It is important to note that, unlike in a subsonic jet, there is no constant velocity or Mach number, in the core region for supersonic jets. This is because of the compression and expansion waves present in the core region. Therefore, it is a common practice to take the supersonic jet core as the axial distance from the nozzle exit, upto which supersonic flow prevails[100]. Shorter the jet core length (that is the reduction in core length caused by the tabs) higher is the mixing promoting capability caused by the tabs. The supersonic length is calculated from the centreline Pitot pressure variation and is the main parameter used to compare the mixing promoting efficiency of the different configurations[58,60,61,69,101].

The centreline decay of uncontrolled jet and the jet controlled with sharp and truncated right-angled triangular tabs, for the highly overexpanded state with p_e/p_a of 0·511, are compared in Fig. 8. The centreline Pitot pressure decay caused by rectangular tabs is also shown in this plot. The core length for the uncontrolled jet is about $6{\cdot}6D_e$. The characteristic decay for the uncontrolled jet continues upto around $20D_e$. When rectangular tabs are placed at the nozzle exit, jet core goes up to $7{\cdot}3D_e$. That is, the control abates the mixing. But, the waves prevailing in the core of the jet

https://doi.org/10.1017/S0001924000009969 Published online by Cambridge University Press

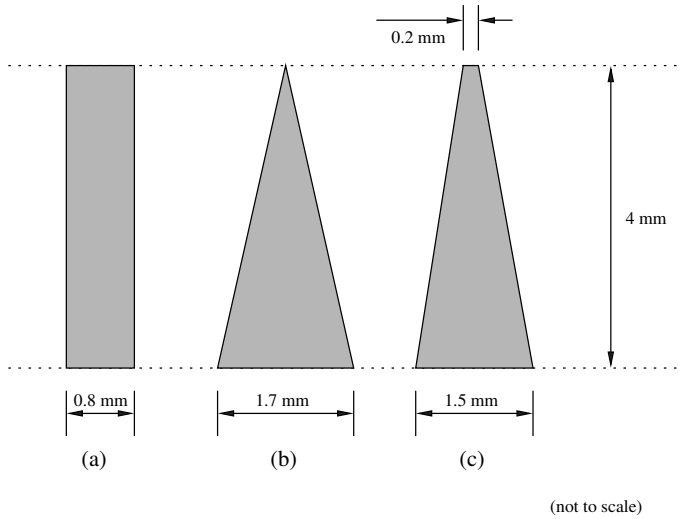

Figure 7. Schematic representation of different tab geometries (a) rectangular tab, (b) isosceles trian- gular with sharp vertex tab and (c) isosceles triangular with truncated vertex tab; The uncertainty inmeasurement was ±0·02mm.

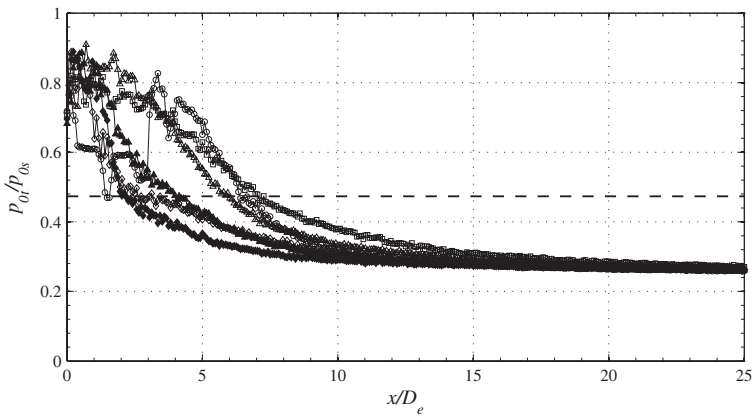

Figure 8. Comparison of centreline total pressure behind local normal shocks of the highly overexpanded jet with p_e/p_a = 0·511; ○ - Uncontrolled jet, □ - Jet controlled with rectangular tabs, Δ - Jet controlled with sharp vertex right-angled triangular tabs, ◊ - Jet controlled with truncated vertex right-angled triangular tabs, ▲ - Jet controlled with sharp vertex isosceles triangular tabs, and ♦ - Jet controlled with truncated vertex right-angled triangular tabs; The dotted line shows the cut-off pressure ratio for the supersonic core length as given in Table 2.

controlled with rectangular tabs are weaker than the uncontrolled jet, as seen from the reduced Pitot pressure values. When the sharp vertex right-angled triangular tabs are placed at the nozzle exit, there is only a marginal reduction in core length to that of uncontrolled jet, which is about $6{\cdot}1D_e$, and the jet becomes fully developed (self- similar profile) as early as $15D_e$. But when the vertex of the right-angled triangular tab is truncated, the core length drastically comes down drastically to about $3{\cdot}4D_e$, which corresponds to a reduction of about 48%. Further the characteristic decay for the truncated right-angled triangular tab is the steepest and the jet becomes fully developed as early as $10D_e$. An important feature to be noted is that in the present investigation, triangular tabs

https://doi.org/10.1017/S0001924000009969 Published online by Cambridge University Press

of right-angled geometry was studied. Recent study in modifying the geometry of the triangular tabs, isosceles triangular tabs (Fig. 7) of identical conditions (geometry and flow parameters) was studied by Arun Kumar and Rathakrishnan[71], were they reported a core length reduction of about 65%, for the jet controlled with truncated isosceles triangular tab. The centreline pressure decay caused by isosceles triangular tabs with sharp and truncated vertex are also shown in this plot. The core length for the isosceles triangular tabs with sharp and truncated vertex are about $4{\cdot}3D_e$ and $2{\cdot}3D_e$, respectively. From these results, it can be brought out that, truncating the vertex of the triangular tab is highly beneficial in promoting mixing than sharp vertex tabs. Moreover, isosceles triangular tabs are superior than right-angled triangular tabs, irrespective of sharp or truncated vertex. From these results it is obvious that, the mixing promoting performance of truncated vertex isosceles triangular tab is the best among the tabs considered.

For the marginally underexpanded state with $p_e/p_a = 1{\cdot}022$, the core length for the uncontrolled jet extends upto about $24{\cdot}2D_e$, as seen in Fig. 9. The core length for the sharp and truncated vertex right-angled triangular tabs respectively are $9{\cdot}4D_e$ and $5{\cdot}4D_e$. That is, a core length reduction of about 61% and 78% are achieved with the sharp and truncated tabs, respectively. These reductions are much lower than the reduction reported for isosceles triangular tabs by Arun Kumar and Rathakrishnan[71], of about 84% and 87% reduction in core length for the sharp and truncated tabs, at same Mach number and expansion ratio. Moreover, the waves in the core of the jet are made weaker by the tabs, as seen by the reduced Pitot pressure oscillations when compared to the uncontrolled jet. In the presence of almost favourable pressure gradient also ($p_e > p_a$), the tabs are found to perform well (Fig. 9). The performance of truncated isosceles triangular tab is once again the best leading to a core length reduction to about $2{\cdot}1D_e$, which is about 87%. The performance of rectangular tab is found to be the least resulting in a core length reduction of about 26%. Results of Munday *et al*[99], for a design jet Mach of 1·5 at almost identical expansion ratio (p_e/p_a= 1·089) is also compared in Fig. 9. This shows that the core length of Mach 1·5 jet is shorter than that of Mach 2·0 jet and also the waves are much weaker for Mach 1·5 jet than Mach 2·0 jet.

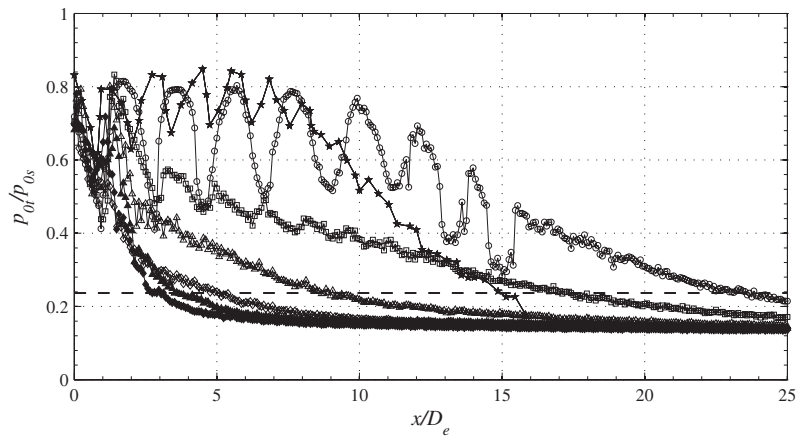

Figure 9. Comparison of centreline total pressure behind local normal shocks of the marginally underexpanded jet with p_e/p_a = 1·022; ○ - Uncontrolled jet, □ - Jet controlled with rectangular tabs, Δ - Jet controlled with sharp vertex right-angled triangular tabs, ◊ - Jet controlled with truncated vertex right-angled triangular tabs, ▲ - Jet controlled with sharp vertex isosceles triangular tabs, and ♦ - Jet controlled with truncated vertex right-angled triangular tabs, * - M_d = 1·5, p_e/p_a = 1·09 (Munday *et al*[99]); The dotted line shows the cut-off pressure ratio for the supersonic core length as given in Table 2.

https://doi.org/10.1017/S0001924000009969 Published online by Cambridge University Press

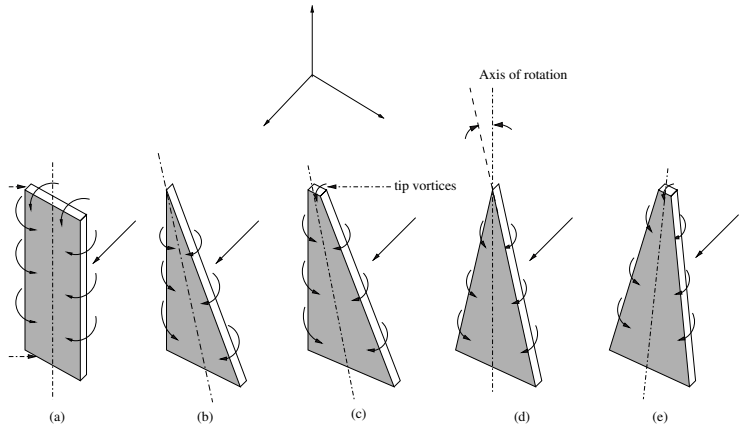

Figure 10. Schematic representation of vortex formation from (a) rectangular tab, (b) right-angled triangular with sharp vertex tab, (c) isosceles triangular with sharp vertex tab, (d) right-angled triangular with truncated vertex tab, and (e) isosceles triangular with truncated vertex tab.

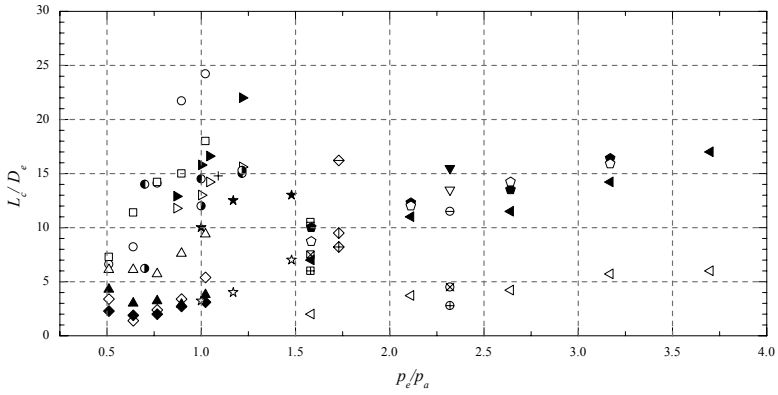

Figure 11. Variation of supersonic core length with expansion ratios (p_e/p_a); ○ - Uncontrolled jet, □ - Jet controlled with rectangular tabs, Δ - Jet controlled with sharp vertex right-angled triangular tabs, ◊ - Jet controlled with truncated vertex right-angled triangular tabs; ⊖ - no control, ⊗ - rectangular tabs and ⊕ - delta tabs (Zaman *et al*[61], M_d = 1·0); ▼ - no control, and ▽ - grooves (Krothapalli *et al*[28], M_d = 1·0); ⊟ - no control, ⊠ - microjets with φ_j = 0·02 and ⊞ - microjets with φ_j = 0·04 (Mohammed K Ibrahim *et al*[5], M_d = 1·0); ◂ - no control, and ◁ - rectangular tabs (Shibu Clement and Rathakrishnan[105], M_d = 1·0); ⬢ - no control, and ⬡ - square grooves (Mrinal *et al*[37], M_d = 1·0); ⟐ - no control, ⟠ - rectangular tabs, and ⊕ - rotating rectangular tabs (Mohammed K Ibrahim., and Yoshiaki Nakamura[106], M_d = 1·35); ★ - no control, and ☆ - rectangular tabs (Samimy *et al*[58], M_d = 1·35); + - no control (Munday *et al*[99], M_d = 1·5); ▸ - no control, and ▷ - rectangular tabs (Chiranjeevi and Rathakrishnan[102], M_d = 1·8); ◐ - no control, and ◑ - square grooves (Vishnu and Rathakrishnan[36] M_d = 1·8); ▲ - delta tabs with sharp vertex, and ♦ - delta tabs with truncated vertex (Arun Kumar and Rathakrishnan[71], M_d = 2·0).

A closer look into the flow physics of the momentum transfer process associated with the small scale vortices shed from the tab would explain the reason for its mixing promoting superiority. It is well known that the vortices shed from an object is proportional to the half-width of the object normal to the stream direction[70]. For the rectangular tab the half-width is uniform all along the tab length from the root end to the tip end. Therefore the tab would shed mixing promoting vortices of only uniform size all along its edges, excepting the tip where there are are two sharp corners

https://doi.org/10.1017/S0001924000009969 Published online by Cambridge University Press

and the vortices shed from the flat tip end and side wall are of different size and would interact intensely (Fig. 10). Also, the vortices shed from the tip would be of transverse type (y-direction), whereas those shed from the edges were are normal type (z-direction). Therefore, the uniform vortices shed by the rectangular tab would travel some downstream distance before becoming active in promoting mixing. Whereas, the triangular tab owing to its geometry would shed vortices of continuously varying size all along its edges, with larger at the root end and continuously decreases toward the tip end. The isosceles triangular tab, capable of shedding vortices of continuously varying size along its edges, at every height from the base would be of identical size, though of opposite family. But, the mixing promoting vortices shed from the right-angled triangular tab would be of different size at all height, in addition to being of opposite family (Fig. 10). Moreover, the vortices of continuously varying size shedding from the opposite sides of isosceles triangular tab are inclined at equal angle (ϕ) with respect to the axis of the tab. But the vortices from the opposite edges of the right-angled triangular tab are inclined with respect to the tab axis at different angles (ϕ). These combinations; continuously varying size of vortices of opposite family, with their axes at unequal inclination to the tab axis might be the reason of reduced mixing promoting efficiency of the right-angled triangular tab compared to the isosceles triangular tab. Another important feature to be noted is that near the sharp vertex tip, though the vortices are of different size and opposite family, their closer proximity would make them to interact intensely leading to loss of vorticity content. This might be the reason of reduced mixing promoting efficiency of the sharp vertex triangular tab compared to the truncated vertex triangular tab. When the vertex is truncated, even at the tip, vortices of opposite family do not interact among themselves. This might be an advantage because almost entire vorticity content available with the mixing promoting vortices would be used for mixing promotion[71]. This can be regarded as the primary reason of the better efficiency of the triangular tab with truncated vertex than the sharp vertex. However, the mixing promoting efficiency of sharp triangular tab is higher than the rectangular tab due to the mixed size of vortices shed from the triangular tab.

From the centreline pressure decay plots (Figs 8 and 9) it is evident that the mixing promotion caused by right-angled triangular tabs are significantly lower than that for isosceles triangular tab. Moreover, truncating the vertex of the tab is found to be of immense benefit in mixing promotion at all the three zones.

3.2.3 Variation of core length

The variation of non-dimensionalised core length (L_c/D_e) with the expansion ratio (p_e/p_a), for the uncontrolled and controlled jets are shown in Fig. 11. For the uncontrolled jet and the rectangular tabs, the core length shows a monotonic increases with increase in expansion ratio, but for the triangular tabs with sharp and truncated vertex, there is no such variation in core length with expansion ratio. The core length for the rectangular tab is the highest among the tabs studied, implying the least mixing promoting efficiency, at all the expansion ratios of the present investigation. That is, the performance of triangular tabs are superior than the rectangular tabs, at all levels of expansion. Zaman *et al*[61], also observed that the triangular tabs performs better than rectangular tab. The core length variation of isosceles triangular tabs with sharp and truncated vertex, studied by Arun Kumar and Rathakrishnan[71], are also shown in Fig. 11. Among the triangular tabs studied, the core length for the truncated isosceles triangular tabs is the lowest, implying maximum mixing promoting efficiency. Moreover, the performance of isosceles triangular tabs are better than the right-angled triangular tabs, at both sharp and truncated vertex all all levels of expansion. A point to be noted is that, the core length of isosceles triangular tabs with sharp and truncated vertex are less than $5D_e$, at all levels of expansion of the present study.

https://doi.org/10.1017/S0001924000009969 Published online by Cambridge University Press

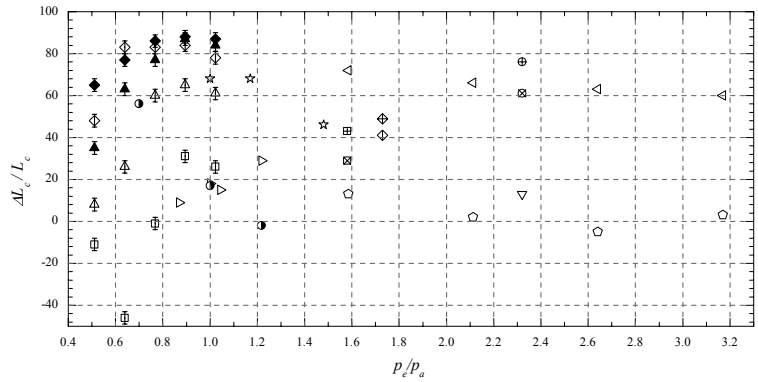

Figure 12. Variation of percentage reduction in supersonic core length with uncontrolled jet; □ - Jet controlled with rectangular tabs, Δ - Jet controlled with sharp vertex right-angled triangular tabs, ◊ - Jet controlled with truncated vertex right-angled triangular tabs; ⊗ - rectangular tabs and ⊕ - delta tabs (Zaman *et al*[61], M_d = 1·0); ▽ - grooves (Krothapalli *et al*[28], M_d = 1·0); ⊠ - microjets with ϕ_j = 0·02 and ⊞ - microjets with ϕ_j = 0·04 (Mohammed K Ibrahim et al[5], M_d = 1·0); ◁ - rectangular tabs (Shibu Clement and Rathakrishnan[105], M_d = 1·0);○- square grooves (Mrinal *et al*[37], M_d = 1·0); ⊕rectangular tabs, and ⊕- rotating rectangular tabs (Mohammed K Ibrahim., and Yoshiaki Nakamura[106], M_d = 1·35); ☆ - rectangular tabs (Samimy *et al*[58], M_d =1·35); ▷ - rectangular tabs (Chiranjeevi and Rathakrishnan[102], M_d = 1·8); ◑ - square grooves (Vishnu and Rathakrishnan[36], M_d = 1·8); ▲ - delta tabs with sharp vertex, and ♦ - delta tabs with truncated vertex (Arun Kumar and Rathakrishnan[71], M_d = 2·0).

Results of Samimy *et al*[58], Munday *et al*[99], Chiranjeevi and Rathakrishnan[102] and the present study, at almost identical expansion ratio (p_e/p_a = 1·0) is also compared in Fig.11. It is seen that the core length of the jets increases with increase in design Mach number (M_d). This is because of the reduced jet Mach number (M_j), for the low design Mach number (M_d) jets.

To quantify the effectiveness of the tab in promoting mixing, a parameter named; percentage reduction in core lengh ($\Delta L_c/L_c$) is defined as:

$$\frac{\Delta L_c}{L_c} = \frac{(L_c)_{\text{uncontrolled jet}} - (L_c)_{\text{controlled jet}}}{(L_c)_{\text{uncontrolled jet}}} \quad \ldots (5)$$

The variation of percentage reduction in core length ($\Delta L_c/L_c$) with expansion ratio (p_e/p_a) is shown in Fig. 12. It is seen that the performance of the right-angled triangular tab with sharp and truncated vertex is the best when compared to rectangular tabs. However, among the right-angled triangular tabs, the truncated vertex is found to the best than the sharp vertex. From these results it evident that, truncating the vertex of the right-angled triangular tab is found to perform better than the sharp vertex right-angled triangular tab. This kind of similar observation was also reported by Arun kumar and Rathakrishnan[71] for the isosceles triangular tab at identical conditions. The overall performance of isosceles triangular tab is higher than the right-angled triangular tab, at both sharp and truncated vertex. This cross-plot clearly demonstrates the superiority of isosceles triangular tabs over right triangular tabs. An interesting feature found in Fig. 12 is that, the triangular tabs are found to be most efficient at moderately overexpanded stat with p_e/p_a = 0·895. This kind of observation was also reported by Arun Kumar and Rathakrishnan[71,103,104]. From this discussion, we can infer that the effectiveness of jet mixing is strongly dictated by the expansion level and shape of the tab.

The core length of uncontrolled and controlled jet and percentage reduction in core reduction of controlled jets over uncontrolled jets at different expansion ratios are tabulated in Table 3.

https://doi.org/10.1017/S0001924000009969 Published online by Cambridge University Press

Table 3
Supersonic core length (L_c/D_e) of the jet at different expansion ratios (p_e/p_a)

p_e/p_a	0·511	0·639	0·767	0·895	1·022
Uncontrolled jet	6·6	8·2	14·1	21·7	24·2
Rectangular tabs	7·3	12·0	14·2	15·0	18·0
Sharp vertex right-angled triangular tabs	6·1	6·1	5·7	7·6	9·4
Truncated vertex right-angled triangular tabs	3·4	1·4	2·4	3·4	5·4
Sharp vertex isosceles triangular tabs[71]	4·3	3·0	3·2	2·9	3·8
Truncated vertex isosceles triangular tabs[71]	2·3	1·9	2·0	2·7	3·1

As seen from Fig. 12, Samimy *et al*[58], reported that around 68% reduction in core length was achieved for square tabs at p_e/p_a almost 1·0. However, in the present study at identical expansion ratio, a core length reduction of about 26% was achieved for rectangular tabs. A point to be noted is that, it is well known that performance of a tab increases with increase in blockage. Inspite of 5% tab blockage in the present study the reduction in core length is much lower when compared to 3% tab blockage of Samimy *et al*[58]. This might be because of the higher jet Mach number (M_j = 2·01), for the present study than the study by Samimy *et al*[58] (M_j = 1·35). Even-though the core length reduction caused by the rectangular tabs is lower than the results of Samimy *et al*[58], but the core length of the jet controlled by the triangular tabs are the maximum. An interesting feature to be noticed is that, the performance of tabs are found to higher than the performance of microjet injection (Mohammed K Ibrahim *et al*[5]). That is, at identical jet Mach number (M_j = 1·36) and expansion ratio (p_e/p_a = 1·59) for the design Mach number (M_d = 1·0), the percentage reduction in core length for the jet controlled with microjet injection [5] is around 43%, but for the jet controlled with tabs, as high as 72% reduction in core length was achieved[105]. However, a point to be noted is that the thrust loss is significant in the presence of tabs. Whereas, the thrust loss in microjet is only less than 0·05%[13]. The core length reduction for the jet controlled by tabs (Zaman *et al*[61]) are much higher than that of the jet controlled by grooves (Krothapalli *et al*[28]) at identical jet Mach number (M_j = 1·63), design Mach number (M_d = 1·0) and expansion ratio (p_e/p_a = 2·35). Also, the core length reduction for the jet controlled by tabs (Shibu and Rathakrishnan[105]) are much higher than that of the jet controlled by grooves (Mrinal *et al*[37]) at identical jet Mach numbers and expansion ratios for the design Mach number (M_d) of 1·0. Moreover, for the design Mach number of 1·8 and at identical jet Mach number and expansion ratio, the core length reduction for the jet controlled by tabs (Chiranjeevi and Rathakrishnan[102]) are much higher than that of the jet controlled by grooves (Vishnu and Rathakrishnan[36]). Thus, from these evidences it can be stated that the, tabs are a better form of control than introducing grooves at the nozzle exit and microjet injection.

3.2.4 Iso-pitot pressure contours

To study the near-field and far-field mixing caused by the uncontrolled and controlled jets, the Pitot pressures were measured in 1mm interval apart in both *y*- and *z*-directions. The measured Pitot pressures p_{0t} were normalised with p_{0s} and plotted in the non-dimensionalised *yz*-plane. Iso-Pitot pressure contours in the non-dimensionalised *yz*-plane at different axial locations from x/D_e = 0·5 to 8 are presented in Figs 13-17, for the moderately overexpanded state with p_e/p_a = 0·895. The iso-Pitot contours for isosceles triangular tabs with sharp and truncated vertex, studied by Arun Kumar and Rathakrishnan[71], are also shown. At the very near field x/D_e = 0·5, as seen in Fig. 13, the circular shape of the nozzle exit is retained for the uncontrolled jet. But,

https://doi.org/10.1017/S0001924000009969 Published online by Cambridge University Press

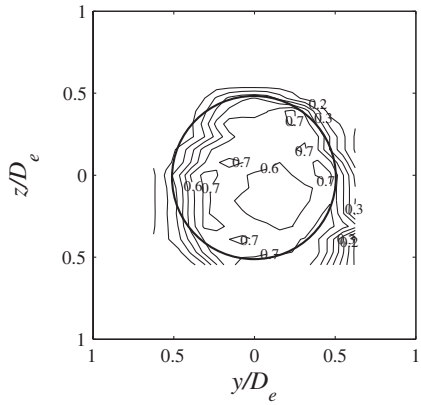

(a) Uncontrolled jet

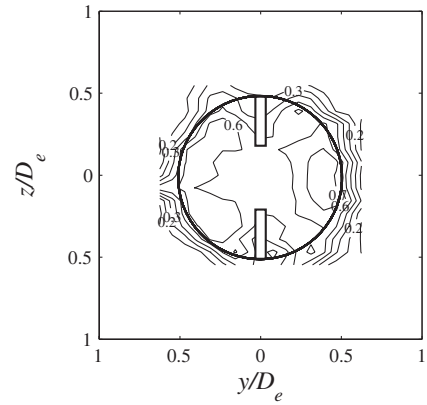

(b) Jet controlled with rectangular tab

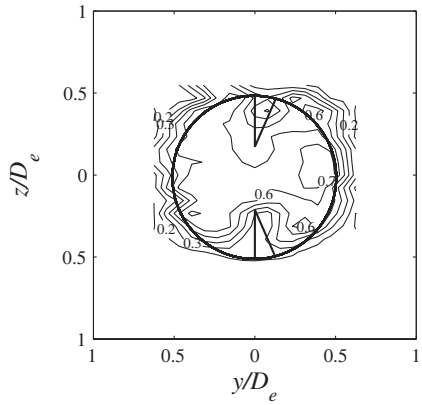

(c) Jet controlled with sharp vertex right-angled triangular tabs

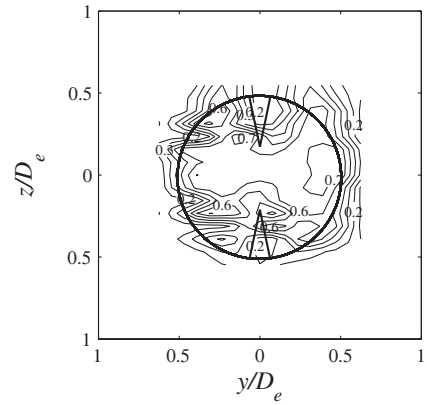

(d) Jet controlled with sharp vertex isosceles triangular tabs

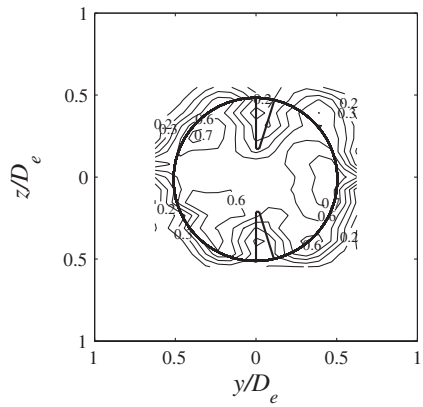

(e) Jet controlled with truncated vertex right-angled triangular tabs

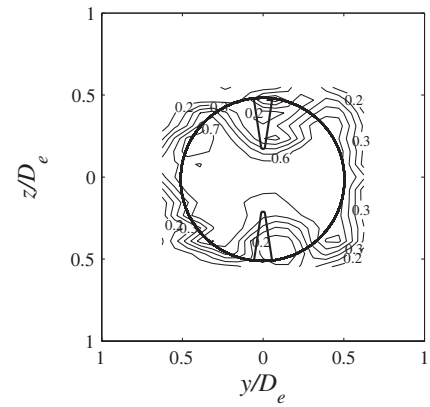

(f) Jet controlled with truncated vertex isosceles triangular tabs

Figure 13. Iso-Pitot (p_{0t} /p_{0s}) contour of the uncontrolled and controlled jets for moderately overexpanded state with p_e/p_a = 0·895 at x/D_e = 0·5.

https://doi.org/10.1017/S0001924000009969 Published online by Cambridge University Press

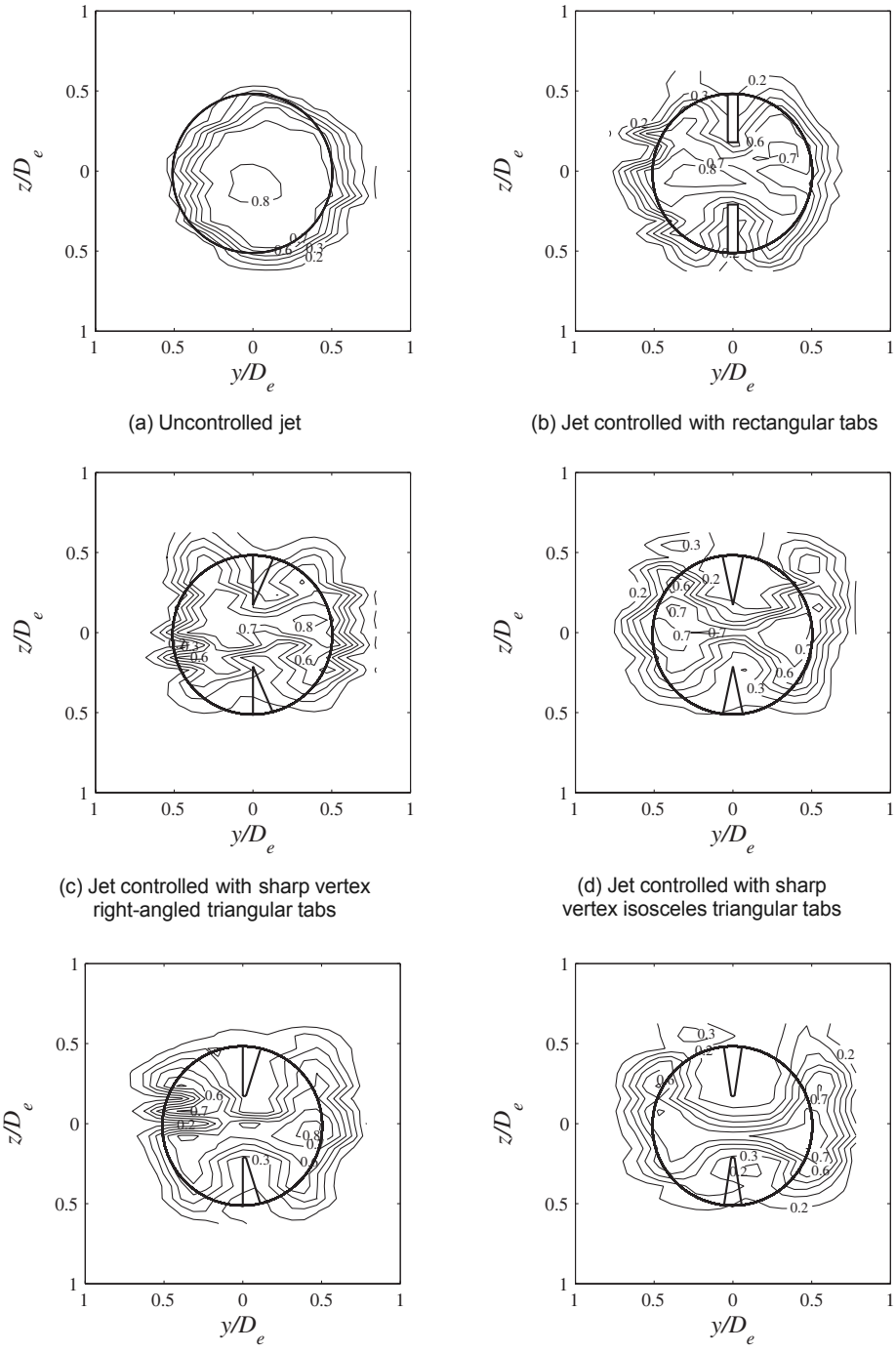

(a) Uncontrolled jet

(b) Jet controlled with rectangular tabs

(c) Jet controlled with sharp vertex right-angled triangular tabs

(d) Jet controlled with sharp vertex isosceles triangular tabs

(e) Jet controlled with truncated vertex right-angled triangular tabs

(f) Jet controlled with truncated vertex isosceles triangular tabs

Figure 14. Iso-Pitot (p_{0t}/p_{0s}) contour of the uncontrolled and controlled jets for moderately overexpanded state with p_e/p_a = 0·895 at x/D_e = 1·0.

https://doi.org/10.1017/S0001924000009969 Published online by Cambridge University Press

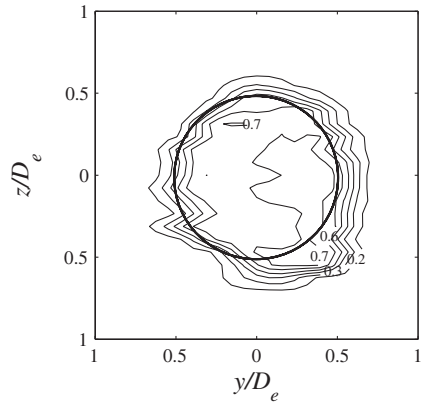

(a) Uncontrolled jet

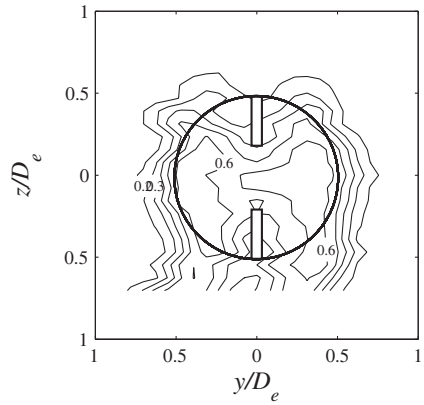

(b) Jet controlled with rectangular tab

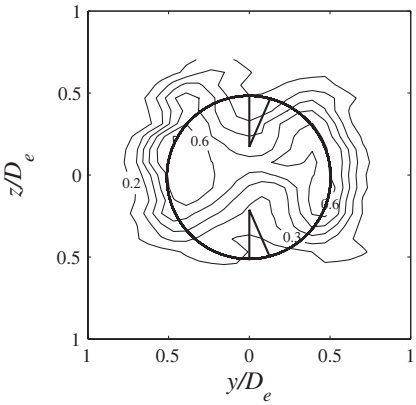

(c) Jet controlled with sharp vertex right-angled triangular tabs

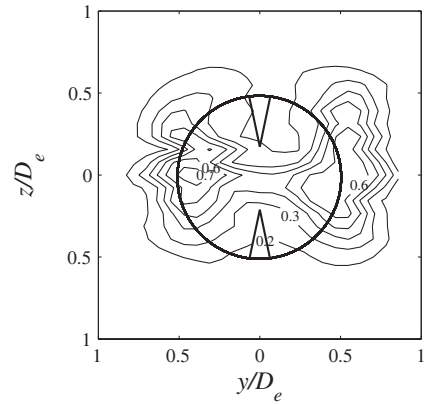

(d) Jet controlled with sharp vertex isosceles triangular tabs

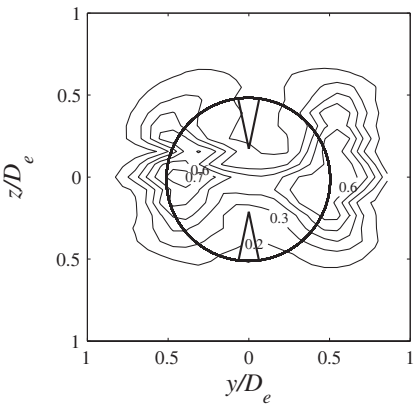

(e) Jet controlled with truncated vertex right-angled triangular tabs

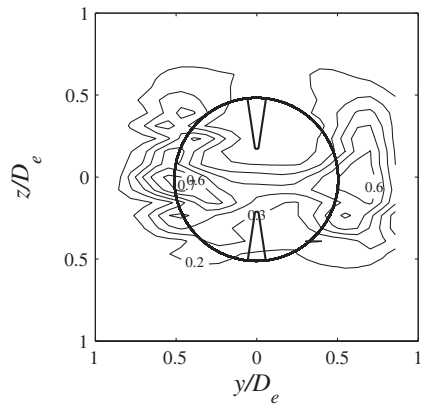

(f) Jet controlled with truncated vertex isosceles triangular tabs

Figure 15. Iso-Pitot (p_{0t} /p_{0s}) contour of the uncontrolled and controlled jets for moderately overexpanded state with p_e/p_a = 0·895 at x/D_e = 2·0.

https://doi.org/10.1017/S0001924000009969 Published online by Cambridge University Press

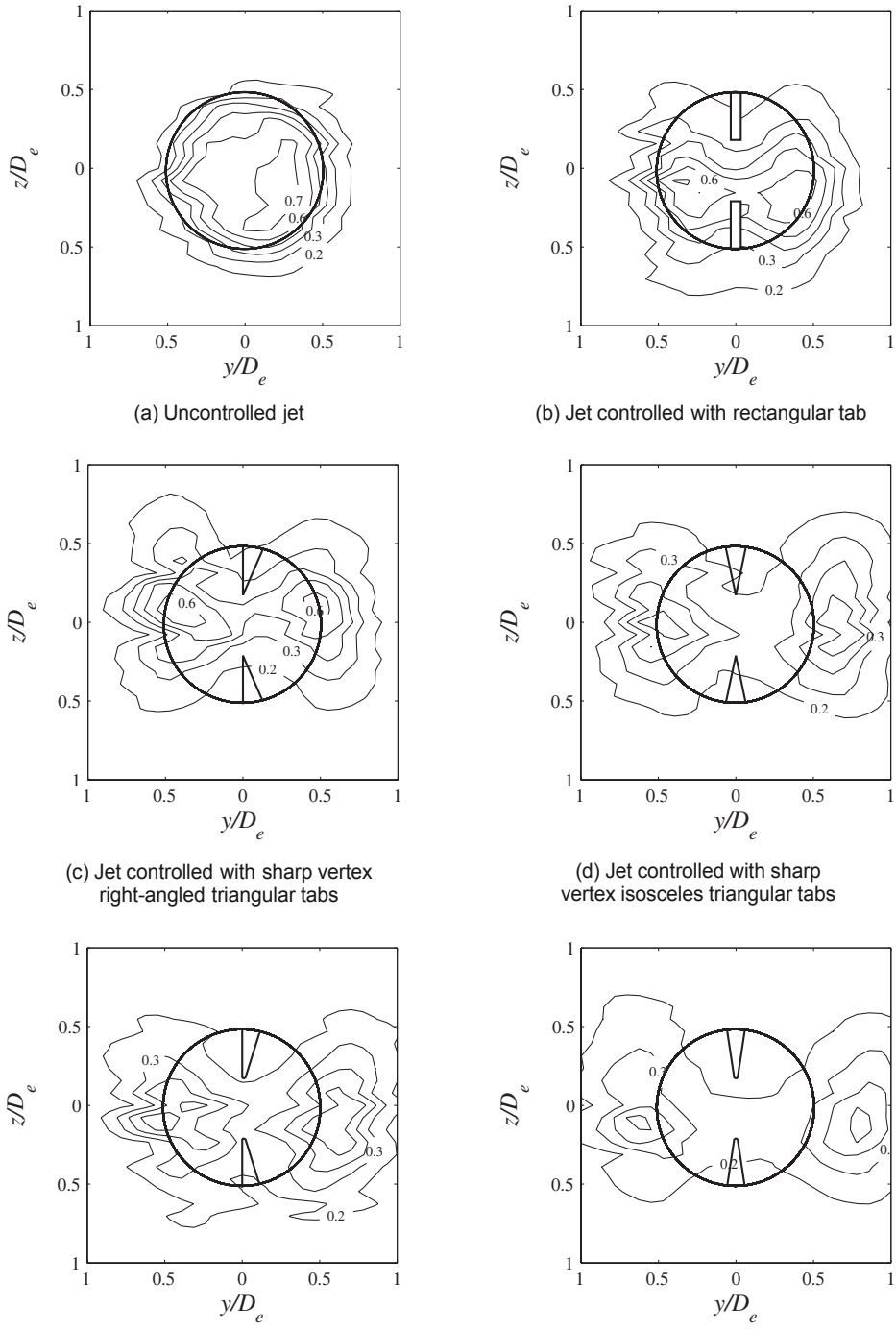

(a) Uncontrolled jet

(b) Jet controlled with rectangular tab

(c) Jet controlled with sharp vertex right-angled triangular tabs

(d) Jet controlled with sharp vertex isosceles triangular tabs

(e) Jet controlled with truncated vertex right-angled triangular tabs

(f) Jet controlled with truncated vertex isosceles triangular tabs

Figure 16. Iso-Pitot (p_{0t}/p_{0s}) contour of the uncontrolled and controlled jets for moderately overexpanded state with p_e/p_a = 0·895 at x/D_e = 4·0.

https://doi.org/10.1017/S0001924000009969 Published online by Cambridge University Press

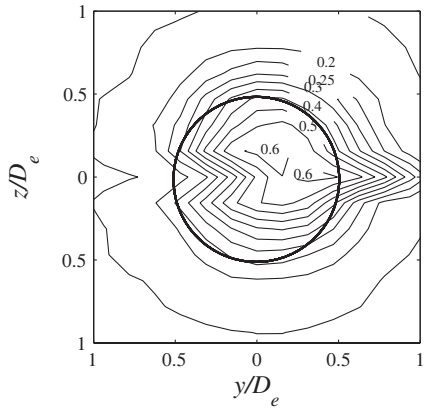

(a) Uncontrolled jet

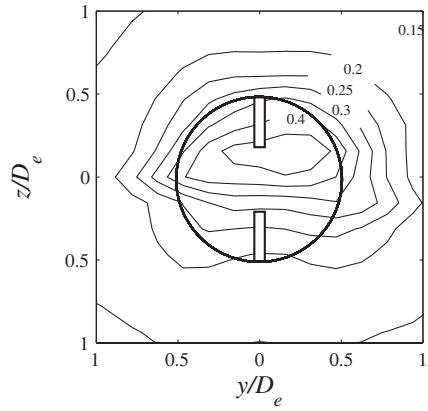

(b) Jet controlled with rectangular tab

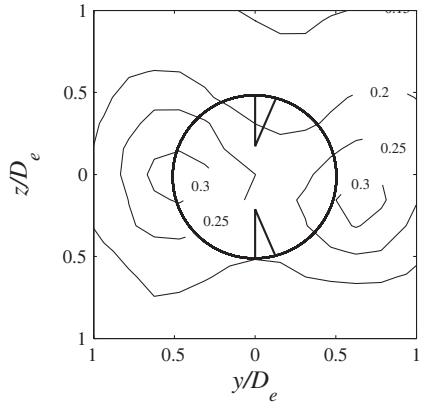

(c) Jet controlled with sharp vertex right-angled triangular tabs

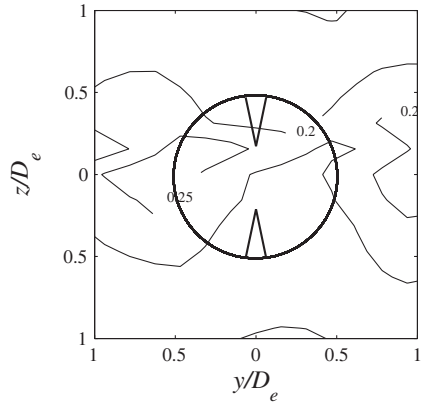

(d) Jet controlled with sharp vertex isosceles triangular tabs

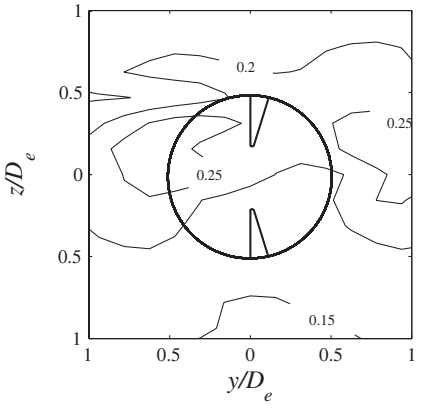

(e) Jet controlled with truncated vertex right-angled triangular tabs

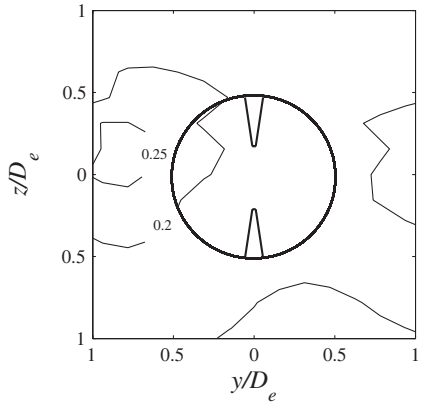

(f) Jet controlled with truncated vertex isosceles triangular tabs

Figure 17. Iso-Pitot (p_{0t} /p_{0s}) contour of the uncontrolled and controlled jets for moderately overexpanded state with p_e/p_a = 0·895 at x/D_e = 8·0.

https://doi.org/10.1017/S0001924000009969 Published online by Cambridge University Press

Table 4
Percentage reduction in core length ($\Delta L_c / L_c$) of the controlled jets against uncontrolled jet at different expansion ratios (p_e/p_a)

p_e/p_a	0·511	0·639	0·767	0·895	1·022
Rectangular tabs	-11	-46	-1	31	26
Sharp vertex right-angled triangular tabs	8	26	60	65	61
Truncated vertex right-angled triangular tabs	48	83	83	84	78
Sharp vertex isosceles triangular tabs[71]	35	63	77	87	84
Truncated vertex isosceles triangular tabs[71]	65	77	86	88	87

the controlled jets shows two pressure peaks on either side of the jet axis, which is taken as an indication of jet bifurcation. With increase of axial distance the spread for both rectangular and triangular tabs are found to increase, as seen in Fig. 14 for $x/D_e = 1$. As we move further to $x/D_e = 2$ (Fig. 15), it is seen that for jet controlled with triangular tabs, spread along y-direction (normal to the tabs) is higher than that along z-direction (along the tabs). Also, for the truncated triangular tabs (Figs 15(e) and 15(f)), the spread along y-direction is significantly larger than that of sharp triangular tabs (Figs 15(c) and 15(d)), which shows the effectiveness of truncated vertex triangular tabs over sharp vertex triangular tabs. With increase of axial distance to $x/D_e = 4$, it is seen that the spread for the truncated triangular tab (Figs 16(e) and 16(f)) in the y-direction is larger than the sharp triangular tab (Figs 16(c) and 16(d)), as reported at $x/D_e = 2$. Moreover, the distortion is higher for the triangular tabs, than that of rectangular tabs. An interesting feature to be noticed is that, the Pitot pressure level (p_{0t}/p_{0s}) of about 0·6 is seen for the rectangular and sharp vertex right-angled triangular tabs. However, for the other triangular tabs the Pitot pressure levels are only about 0·4. Moreover the region covering this Pitot pressure level is higher for the sharp vertex triangular tabs (Figs 16(c) and 16(d)) than the truncated vertex triangular tabs (Figs 16(e) and 16(f)). The spread for the triangular tabs had grown significantly larger than the rectangular tabs at $x/D_e = 8$ (Fig. 17). Also, the region covering the Pitot pressure level with 0·25, is higher for the right-angled triangular tabs (Figs 17(c) and 17(e)) than the isosceles triangular tabs (Figs 17(d) and 17(f)). Throughout the axial location, jet spread for the isosceles triangular tabs in the y-direction is significantly larger than that of right-angled triangular tabs, which shows the effectiveness of isosceles triangular tabs over right-angled triangular tabs. It can also be brought out that the triangular tabs, in the presence of adverse pressure gradient, cause higher spread than the rectangular tab right from the proximity of the nozzle exit. Moreover, these results also explicitly exhibit that the spread for truncated triangular tab continuous to be superior than the sharp triangular and rectangular tabs. From the results of iso-baric contours also, it is evident that, the tab shedding vortices of continuously varying size performs better if the vertex is truncated.

3.2.5 Radial pitot pressure profiles

In order to support the evidences made in centreline Pitot pressure decay and iso-Pitot contours, the pressure profiles for the controlled jets, in the direction along the tabs (z-direction) and normal to the tabs (y-direction), were measured for the all possible combination of the present study. A representative set of pressure profile for the uncontrolled and controlled jet at $p_e/p_a = 0{\cdot}511$ and 0·767 are shown in Figure 18. For a given tab configuration, very little distortion was produced in the highly overexpanded condition as compared to the prominent distortion at marginally overexpanded conditions, corresponding to $p_e/p_a = 0{\cdot}511$ (Figs 18(a),

https://doi.org/10.1017/S0001924000009969 Published online by Cambridge University Press

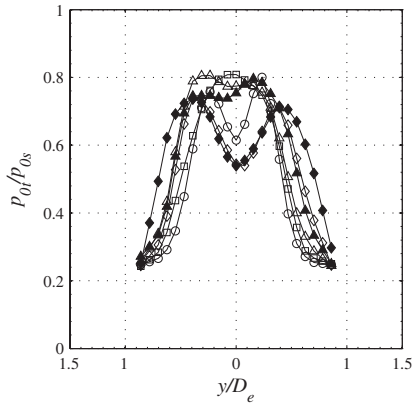

(a) x/D_e = 1·0; p_e/p_a = 0·511

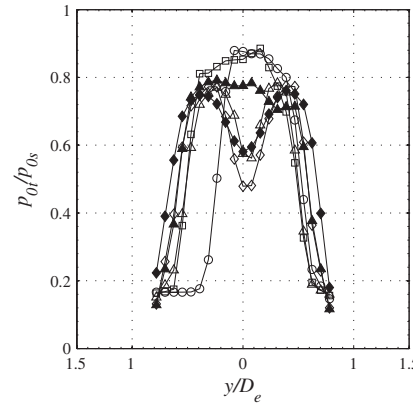

(b) x/D_e = 1·0; p_e/p_a = 0·767

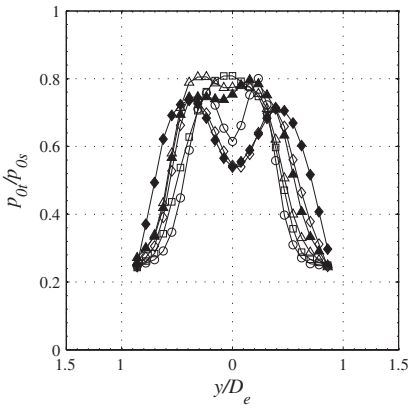

(c) x/D_e = 2·0; p_e/p_a = 0·511

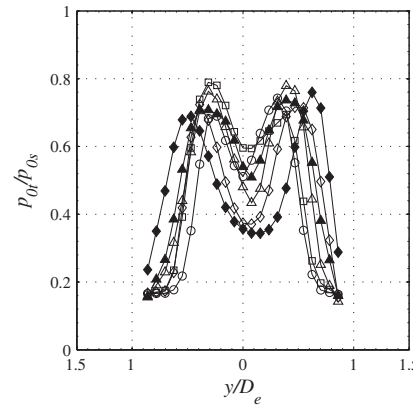

(d) x/D_e = 2·0; p_e/p_a = 0·767

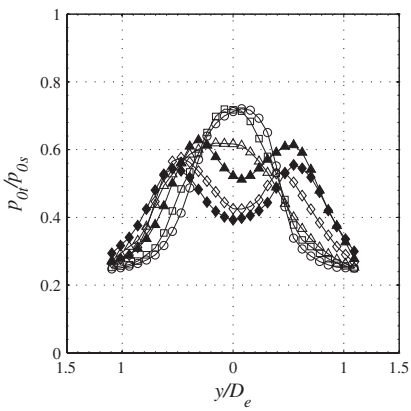

(e) x/D_e = 4·0; p_e/p_a = 0·511

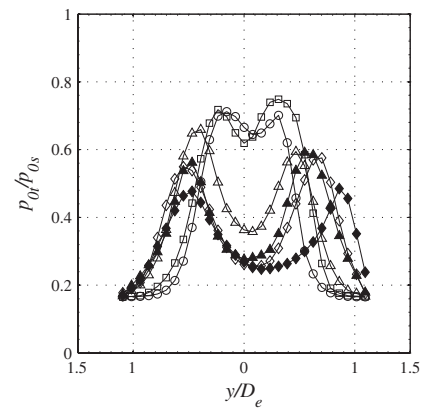

(f) x/D_e = 4·0; p_e/p_a = 0·767

https://doi.org/10.1017/S0001924000009969 Published online by Cambridge University Press

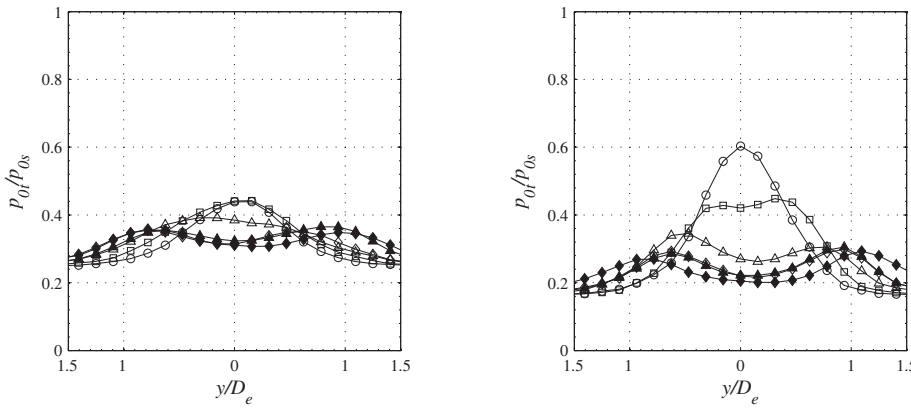

(e) x/D_e = 8·0; p_e/p_a = 0·511 (f) x/D_e = 8·0; p_e/p_a = 0·767

Figure 18. Radial Pitot pressure profiles for the controlled jets; ○ - Uncontrolled jet, □ - Jet controlled with rectangular tabs, Δ - Jet controlled with sharp vertex right-angled triangular tabs, ◊ - Jet controlled with truncated vertex right-angled triangular tabs, ▲ - Jet controlled with sharp vertex isosceles triangular tabs, and ♦ - Jet controlled with truncated vertex right-angled triangular tabs.

18(c), 18(e) and 18(g)) and p_e/p_a = 0·767 (Figs 18(b), 18(d), 18(f) and 18(h)) all axial locations. This kind of observation was also reported by Samimy *et al*[58]. At the near field location of x/D_e = 1·0 at p_e/p_a = 0·511 (Fig. 18(a)), the jet controlled by triangular tabs shows no distortion, whereas at p_e/p_a = 0·767 (Fig. 18(b)), the jet controlled with triangular tabs shows a prominent distortion. However for the jet controlled by rectangular tabs shows no distortion even at p_e/p_a = 0·767. As we move downstream to x/D_e = 2 and 4 at p_e/p_a = 0·511 (Figs 18(c) and 18(e)) and p_e/p_a = 0·767 (Fig. 18(d) and 18(f)), the distortion is higher for the triangular tabs, than that of rectangular tabs. Thus it can be stated that the, triangular tabs exhibit higher distortion of the jet and resultant increase in jet mixing, than the rectangular tabs. Also, for the truncated vertex triangular tabs, the spread along the direction normal to the tabs is significantly larger than that of sharp vertex triangular tabs. For the jet controlled with triangular tabs, the Pitot pressure at the jet centreline (y/D_e = 0) is highest for the sharp vertex right-angled triangular tabs and lowest for the truncated vertex isosceles triangular tabs. Throughout the axial location, jet spread for the isosceles triangular tabs in the *y*-direction is significantly larger than that of right-angled triangular tabs.

A point to be noted is that, the base-width of the triangular tab is same for isosceles and right-angled geometries, for both sharp and truncated vertex. However, the distortion is larger for the isosceles triangular tab than the right-angled triangular tab, for both sharp and truncated vertex. Moreover, the mixing promoting performance of the truncated vertex triangular tabs are higher than the sharp vertex triangular tabs, which also indicates that the tab tip plays a important role. So, it can be brought out that, for a given tab configuration

(*i*) the shape at the tab end has a significant effect on the distortion produced.

(*ii*) with approximately the same flow blockage, it need not be the width alone, but the tab shape also influences the mixing promoting efficiency.

It is seen that, the triangular tabs do not introduce any asymmetry in the direction normal to the tab (*y*-direction). It is also evident that, with increase in axial location the jet spread also increases, which is a typical nature of jet.

https://doi.org/10.1017/S0001924000009969 Published online by Cambridge University Press

4.0 CONCLUSIONS

The results of the present investigation clearly demonstrates that the mixing caused by right-angled triangular tab with truncated vertex is superior than the identical tab with sharp vertex and rectangular tab of equivalent blockage. The mixing promoting efficiency of the tab is found to increase with increase of expansion ratio. At almost perfectly expanded state, core length reduction of about 78% is achieved with truncated right-angled triangular tab, which is lower than the core length reduction of 87%, reported for isosceles triangular tab of identical blockage at same Mach number[71]. It is found that, among the right-angled triangular tabs, the one with truncated vertex is a better mixing promoter. As high as 85% reduction in core length is achieved with truncated right-angled triangular tabs at moderately overexpanded state. The corresponding core length reduction for right-angled triangular tabs with sharp vertex and rectangular tabs are 65% and 30%, respectively. It is found that, inspite of the intense action of the mixing promoting vortices of continuously varying size shed by the triangular tabs, the jet does not become unduly asymmetry. The waves in the rectangular tabs case are found to be stronger than those for the right-angled triangular tabs. The waves present in the jet field controlled by truncated right- angled triangular tab is found to be significantly weaker than the waves prevailing in the jet controlled by sharp right-angled triangular tab and rectangular tab.

REFERENCES

1. GUTMARK, E.J., SCHADOW, K.C. and YU, K.H. Mixing enhancement in supersonic free shear flows, *Annual Review of Fluid Mechanics*, 1995, **27**, (1), pp 375-417.
2. GUTMARK, E.J. and GRINSTEIN, F.F. Flow control with non-circular jets, *Annual Review of Fluid Mechanics*, 1999, **31**, (1), pp 239-272.
3. SEINER, J.M., DASH, S.M. and KENZAKOWSKI, D.C. Historical survey on enhanced mixing in scramjet engines, *J Propulsion and Power*, 2001, **17**, (6), pp 1273-1286.
4. KNOWLES, K. and SADDINGTON, A.J. A review of jet mixing enhancement for aircraft propulsion applications, *Proceedings of the IMechE, Part G: J Aerospace Engineering*, 2006, **220**, (2), pp 103-127.
5. IBRAHIM, M.K., KUNIMURA, R. and NAKAMURA, Y. Mixing enhancement of com- pressible jets by using unsteady microjets as actuators, *AIAA J*, 2002, **40**, (4), pp 681-688.
6. ARAKERI, V.H., KROTHAPALLI, A., SIDDAVARAM., V., ALKISLAR, M.B. and LOURENCO, L.M. On the use of microjets to suppress turbulence in a Mach 0·9 axisymmetric jet, *J Fluid Mechanics*, 2003, **490**, pp 75-98.
7. THOMAS, C., BRA, J.-C. and SUNYACH, M. Noise reduction of a Mach 0·7 - 0·9 jet by impinging microjets, *Comptes Rendus Mcanique*, 2006, **334**, (2), pp 98-104.
8. THOMAS, C., SUNYACH., M., JUV, D. and BERA, J-C. Jet-noise reduction by impinging microjets: An acoustic investigation testing microjet parameters, *AIAA J*, 2008, **46**, (5), pp 1081-1087.
9. DAVIS, M.R. Variable control of jet decay, *AIAA J*, May 1982, **20**, (5), pp 606-609.
10. CHAUVET, N., DECK, S. and JACQUIN, L. Numerical study of mixing enhancement in a supersonic round jet, *AIAA J*, 2007, **45**, (7), pp 1675-1687.
11. CHAUVET, N., DECK, S. and JACQUIN, L. Shock patterns in a slightly underex- panded sonic jet controled by radial injections, *Physics of Fluids*, 2007, **19**, (4).
12. BEHROUZI, P., FENG, T. and MCGUIRK, J.J. Active flow control of jet mixing using steady and pulsed fluid tabs, *Proc. IMechE*, *Part I: J. Systems and Control Engineering*, 2008, **222**, (5), pp 381-391.
13. YU., S.C.M., LIM., K.S. CHAO, W. and GOH, X.P. Mixing enhancement in subsonic jet flow using the air-tab technique, *AIAA J*, 2008, **46**, (11), pp 2966-2969.
14. WAN, C. and YU, S.C.M. Investigation of air tabs effect in supersonic jets, *J Propulsion and Power*, 2011, **27**, (5), pp 1157-1160.
15. KAMRAN, M.A. and MCGUIRK, J.J. Subsonic jet mixing via active control using steady and pulsed control jets, *AIAA J*, 2011, **49**, (4), pp 712-724.
16. WAN, C. and YU, S.C.M. Numerical investigation of the air-tabs technique in jet flow, *J Propulsion and Power*, 2013, **19**, (1), pp 42-49.

17. VIETS, H. Flip-flop jet nozzle, *AIAA J*, 1975, **13**, (10), pp 1375-1379.
18. TAM, C.K.W. and MORRIS, P.J. Tone excited jets, Part V: A theoretical model and comparison with experiment, *J Sound and Vibration*, 1985, **102**, (1), pp 119-151.
19. GOLDSTEIN, M.E. and LEIB, S.J. Nonlinear roll-up of externally excited free shear layers, 1988, *J Fluid Mechanics*, **191**, pp 481-515.
20. PANTON, R.L. Effect of orifice geometry on Helmholtz resonator excitation by grazing flow, *AIAA J*, 1990, **28**, (1), pp 60-65.
21. BOGDANOFF, D.W. Advanced injection and mixing techniques for scramjet combustors, *J Propulsion and Power*, 1994, **10**, (2), pp 183-190.
22. CHANAUD, R.C. Effects of geometry on the resonance frequency of Helmholtz resonator, *J Sound and Vibration*, 1994, (178), **3**, pp 337-348.
23. WILTZE, J.M. and GLEZER, A. Direct excitation of small-scale motions in free shear flows, *Physics of Fluids*, 1998, **10**, (8), pp 2026-2036.
24. PANNU, S.S. and JOHANNESEN, N.H. The structure of jets from notched nozzles, *J Fluid Mechanics*, **74**, (3), pp 515-528.
25. NORUM, T.D. Screech suppression in supersonic jets, *AIAA J*, 1983, **21**, (2), pp 235-240.
26. SMITH, D.J. and HUGHES, T. The flow from notched nozzles in the presence of a free-stream, *Aeronautical J*, 1984, **88**, pp 77-85.
27. WLEZIEN, R.W. and KIBENS, V. Influence of nozzle asymmetry on supersonic jets, *AIAA J*, 1988, **26**, (1), pp 27-33.
28. KROTHAPALLI, A., MCDANIEL, J. and BAGANOFF, D. Effect of slotting on the noise of an axisymmetric supersonic jet, *AIAA J*, 1990, **28**, (12), pp 2136-2138.
29. LONGMIRE, E.K., EATON, J.K. and ELKINS, C.J. Control of jet structure by crown-shaped nozzles, *AIAA J*, 1992, **30**, (2), pp 505-512.
30. YU K.H., SCHADOW, K.C., KRAEUTLE, K.J. and GUTMARK, E.J. Supersonic flow mixing and combustion using ramp nozzles, *J Propulsion and Power*, 1995, **11**, (6), pp 1147-1153.
31. LONGMIRE, E.K. and DUONG, L.H. Bifurcating jets generated with stepped and sawtooth nozzles, *Physics of Fluids*, 1996, **8**, (4), pp 978-992.
32. VERMA, S.B. and RATHAKRISHNAN, E. Mixing enhancement and noise attenuation in notched elliptic slot free jets, *J Turbo and Jet Engines*, 1998, **15**, pp 7-25.
33. VERMA, S.B. and RATHAKRISHNAN, E. An experimental study on the noise characteristics of notched circular-slot jets, *J SOUND and VIBRATION*, 1999, **226**, pp 383-396.
34. VERMA SHASHI BHUSHAN, V.S. and RATHAKRISHNAN, E. Influence of aspect-ratio on the mixing and acoustic characteristics of plain and modified elliptic slot jets, *Aerospace science and technology*, 2003, **7**, pp 451-464.
35. ELANGOVAN, S. and RATHAKRISHNAN, E. Studies on high speed jets from nozzles with internal grooves. *Aeronaut J*, 2004, **108**, pp 43-50.
36. JAYANT, V. and RATHAKRISHNAN, E. Acoustic characteristics of supersonic jets from grooved nozzles. *J Propulsion and Power*, 2004, **20**, (3), pp 520-526.
37. MRINAL, K., THAKUR, P.S. and ETHIRAJAN, R. Studies on the effect of notches on circular sonic jet mixing, *J Propulsion and Power*, 2006, **22**, (1), pp 211-214.
38. ISHII, T., OINUMA, H., NAGAI, K., TANAKA, N., OBA, Y. and OISHI, T. Experimental study on a notched nozzle for jet noise reduction. ASME Paper GT2011-46244, 2011, pp 265-276.
39. ARUN KUMAR, P., VERMA, S.B. and ELANGOVAN. S. Study of jets from rectangular nozzles with square grooves, *Aeronaut J,* 2011, **115**, pp 187-196.
40. MARTIN, J.E. and MEIBERG, E. Numerical investigation of three-dimensionally evolving jets under helical perturbations, *J Fluid Mechanics*, 1992, **243**, pp 457-487.
41. FAROKHI, S., TAGHAVI, R. and RICE, E.J. Effect of initial swirl distribution on the evolution of a turbulent jet, *AIAA J*, 1989, **27**, (6), pp 700-706.
42. NAUGHTON, J.W. and SETTLES, G.S. Experiments on the mixing via streamwise vorticity, Part 1: Optical m, AIAA Paper 92-3459, July 1992.
43. KRAUS, D.K. An experimental investigation of mixing enhancement in a simulated scramjet combustor by use of swirling jets, NASA TM-109246, 1993.
44. NAUGHTON, J.W., CATTAFESTA, L.N. and SETTLES, G.S. An experimental study of compressible turbulent mixing enhancement in swirling jets, *J Fluid Mechanics*, 1997, **330**, pp 271-305.
45. DUTTON, J.C. Swirling supersonic nozzle, *J Propulsion and Power*, 1987, **3**, (4), pp 342-349.
46. JACOBSEN, L.S., SCHETZ, J.A., GALLIMORE, S.D. and OBRIEN, W. F., Mixing enhancement by jet swirl in

https://doi.org/10.1017/S0001924000009969 Published online by Cambridge University Press

a multiport injector array in supersonic flow, 3rd American Society of Mechanical Engineers/Japanese Society of Mechanical Engineers, Fluids Engineering Summer Meeting, Paper 99-7248, 1999.
47. BRYAN, C., GUTMARK, E.J. and MARTENS, S. Far-field acoustic investigation into chevron nozzle mechanisms and trends, *AIAA J*, 2005, **43**, (1), pp 87-95.
48. UZUN ALI, U. and HUSSAINI, M.Y. Noise generation in the near-nozzle region of a chevron nozzle jet flow, 13th AIAA/CEAS Aeroacoustics Conference, AIAA Paper 3596 2007).
49. CALLENDER, B., GUTMARK, E. and MARTENS, S. Near-field investigation of chevron nozzle mechanisms, *AIAA J*, 2008, **46**, (1), pp 36-45.
50. SCHLINKER, R.H., SIMONICH, J.C., SHARON, D.W., REBA, R.A., COLONIUS, T., GUDEMENDSSON, K. and LADEINCLA, F. Supersonic jet noise from round and chevron nozzles: Experimental studies, 30th AIAA Aeroacoustics Conference, AIAA Paper 3257 (2009).
51. ZAMAN, K.B.M.Q., BRIDGES, J.E and HUFF, D.L. Evolution from 'Tabs' to 'Chevron Technology' a Review, Proceedings of the 13th Asian Congress of Fluid Mechanics, 17-21 December 2010, Dhaka, Bangladesh.
52. RASK, O., KASTNER, J. and GUTMARK, E. Understanding how chevrons modify noise in supersonic jet with flight effects, *AIAA J*, 2011, **49**, (8), pp 1569-1576.
53. MUNDAY, D., HEEB, N., GUTMARK, E., LIU, J. and KAILASANATH, K. Acoustic effect of chevrons on supersonic jets exiting conical convergent-civergent nozzles, *AIAA J*, 2012, **50**, pp 2336-2350.
54. BRADBURY, L.J.S. and KHADEM, A.H. The distortion of a jet by tabs, *J Fluid Mechanics*, 1975, **70**, (4), pp 801-813.
55. AHUJA, K.K. and BROWN, W.H. Shear flow control by mechanical tabs, AIAA Paper 89-0994, 1989.
56. AHUJA, K.K. Mixing enhancement and jet noise reduction through tabs plus ejectors, AIAA Paper 93-4347, 1993.
57. SAMIMY, M., REEDER, M. and ZAMAN, K. Supersonic jet mixing enhancement by vortex generations, AIAA Paper 91-2263, 1991.
58. SAMIMY, M., ZAMAN, K.B.M.Q. and REEDER, M.F. Effect of tabs on the flow and noise field of an axisymmetric jet, *AIAA J*, 1993, **31**, (4), pp 609-619.
59. ZAMAN, K.B.M.Q., REEDER, M.F. and SAMIMY, M. Supersonic jet mixing enhancement by delta-tabs, AIAA Paper 92-3548, 1992.
60. ZAMAN, K. B. M. Q. Streamwise vorticity generation and mixing enhancement in free jets by delta-tabs, AIAA Paper 93-3253,1993.
61. ZAMAN, K.B.M.Q., REEDER, M.F. and SAMIMY, M. Control of an axisymmetric jet using vortex generators, *Physics of Fluids,* 1994, **6**, pp 778-793.
62. REEDER, M.F. and ZAMAN, K.B.M.Q. The impact of tab location relative to the nozzle exit on jet distortion, AIAA 94-3385, 1994.
63. REEDER, M.F and ZAMAN, K.B.M.Q. Impact of tab location relative to the nozzle exit on jet distortion, *AIAA J*, 1996, **34**, (1), pp 197-199.
64. REEDER, M. F. and SAMIMY, M. The evolution of a jet with vortex generating rabs: Real-time visualization and quantitative measurements, *J Fluid Mechanics*, 1996, **311**, pp 73-118.
65. BOHL, D. and Foss, J.F. Characteristic of the velocity and streamwise vorticity fields in a developing tabbed jet, AIAA Paper 95-0102, 1995.
66. BOHL, D. and Foss, J.F. Enhancement of passive mixing tabs by the addition of secondary tabs, AIAA Paper 96-054, 1996.
67. ZAMAN, K.B.M.Q. Axis-switching and spreading of an asymmetric jet: The role of coherent structure dynamics, *J Fluid Mechanics*, 1996, **316**, pp 1-27.
68. STEFFEN, C.J., REDDY. D.R. and ZAMAN, K.B.M.Q. Numerical modeling of jet entrainment for nozzles fitted with delta tabs, AIAA Paper 97-0709, 1997.
69. RATHAKRISHNAN, E. Experimental studies on the limiting tab, *AIAA J*, 2009, **47**, (10), pp 2475-2485.
70. TAKAMA Y, SUZUKI K and RATHAKRISHNAN E. Visualization and size measurement of Vortex shed by flat and arc plates in a uniform flow, *Int Review of Aerospace Engineering*, 2010, **1**, pp 55-60.
71. ARUN KUMAR P. and RATHAKRISHNAN, E. Truncated triangular tabs for supersonic jet control, *J Propulsion and Power*, 2013, **29**, (1), pp 50-65.
72. PARVIZ, B. and MCGUIRK, J.J. Experimental studies of tab geometry effects on mixing enhancement of an axisymmetric jet, *JSME international J. Series B, Fluids and Thermal Engineering*, 1998, **41**, (4), pp 908-917.
73. PARVIZ, B. and MCGUIRK, J.J. Effect of tabs parameter on near field jet plume develop- ment, *J Propulsion and Power*, 2006, **22**, (3), pp 576-585.

74. MI, J. and NATHAN, G.J. Effect of small vortex-generators on scalar mixing in the developing region of a turbulent jet, *Int J Heat and Mass Transfer*, 1999, **42**, pp 3919-3926.
75. ZAMAN, K.B.M.Q. Spreading characteristics of compressible jets from nozzles of various geome- tries, *J Fluid Mechanics*, 1999, **383**, pp 197-228.
76. ZAMAN, K.B.M.Q. Jet spreading increase by passive control and associated performance penalty, AIAA Paper 99-3505, 1999.
77. HARPER-BOURNE, M. and FISHER, M.J. The noise from shock waves in supersonic jets, *Noise mechanisms*, 1974, **131**, pp 1-11.
78. SHAPIRO, A.H. *The dynamics and thermodynamics of compressible fluid flow*, **1**, The Ronald Press Company, 1953.
79. LADENBURG, R.W. (Ed). Physical measurements in gas dynamics and combustion: High speed aerodynamics and jet propulsion, Volume IX. Princeton University Press, 1954.
80. TROPEA, C., YARIN, A.L. and Foss, J.L. (Eds). *Springer handbook of experimental fluid mechanics*, Springer, 2007.
81. CHUE, S.H. Pressure probes for fluid measurement, *Progress in Aerospace Sciences*, 1975, **16**, pp 147-223.
82. KATANODA, H., MIYAZATO, Y., MASUDA, M. and MATSUO, K. Pitot pressures of correctly expanded and underexpanded free jets from axisymmetric supersonic nozzles, *ShockWaves*, 2000, **10**, pp 95-101.
83. ZHANG, XIWEN, PENGFEI, H.A.Q. and ZHAOHUI, Y.A.O. The measurement error analysis when a pitot probe is used in supersonic air flow, *Science China Physics*, *Mechanics and Astronomy*, 2011, **54**, pp 690-696.
84. TAYLOR, J.R. *An Introduction to Error Analysis; The Study of Uncertainties in Physical Measurements*, University Science Books, 1996.
85. BEVINGTON, P.R. *Data Reduction and Error Analysis for the Physical Sciences*, McGraw-Hill Book Company, 1969.
86. MOFFAT, R.J. Contributions to the theory of single-sample uncertainty analysis, 1982, *J Fluids Engineering*, **104**, pp 250-258.
87. MOFFAT, R.J. Using uncertainty analysis in the planning of an experiment. *J Fluids Engineering*, 1985, **107**, pp 173-178.
88. MOFFAT, R.J. Describing the uncertainty in experiment results, *Experimental Thermal and Fluid Sciences*, 1988, **1**, pp 3-17.
89. ARUN KUMAR, P. Triangular Tabs for Supersonic Jet Control, PhD Thesis, 2013, Indian Institute of Technology Kanpur, India.
90. ASHRATOV, E.A. Calculations of axisymmetric jet leaving a nozzle at jet pressure lower than pressure in medium, 1966, *Fluid Dynamics (*translated from Russian), **1**, p 113.
91. STERNBERG, J., Triple-shock-wave interactions, *The Physics of Fluids*, 1959, **2**, pp 179-206.
92. CHOW, W.L. and CHANG I.S. Mach reflection from overexpanded nozzle flows, *AIAA J*, **10**, (9), 1972 pp 1261-1263.
93. CHOW, W.L. and CHANG, I.S. Mach reflection associated with over-expanded nozzle free jet flows, *AIAA J*, **13**, (6), pp 762-766.
94. LI, H. and BEN-DOR, G. Mach reflection wave configuration in two-dimensional supersonic jets of overexpanded nozzles, *AIAA J*, **36**, (3), pp 488-491.
95. PHALNIKAR, K.A. and KUMAR, R. and ALVI, F.S., Experiments on free and impinging supersonic micro-jets, *Experiments in Fluids*, 2008, **44**, pp 819-830.
96. ANDERSON, A.R. and JOHNS, F.R. Nondimensional characteristics of free and deflected supersonic jets exhausting into quiescent air, Technical report, U.S. Naval Air Development Centre, Johnsville, USA, Pa.NADC-ED-5401, ASTIA AD 36,625, 1954
97. ABRAMOVICH, G.N. Theory of turbulent jets (Russian, Moscow, 1960, English translation by the US Air Force Systems Command, Foreign Tech. Div, Technical Documents Liaison Office, MCL 3256, ASTIA AD 283, 858, 1962.
98. SNEDEKER, R.S. and DONALDSON, C. duP, Experiments on free and impinging underexpanded jets from a convergent nozzle, Aeronautical Research Associates of Princeton, Inc, ARAP Kept. 63, DDC 461,622, 1964.
99. MUNDAY, D., GUTMARK, E., LIU, J. and KAILASANATH, K. Flow structure and acoustics of supersonic jets from conical convergent-divergent nozzles, *The Physics of Fluids*, 2011, **23**.
100. RATHAKRISHNAN, E. *Applied gas dynamics*, John Wiley, NJ, USA, 2010.
101. KROTHAPALLI, A., HSIA, Y., BAGANOFF, D. and KARAMCHETI, K. The role of screech tones in mixing of an underexpanded rectangular jet, *J Sound and Vibration*, 1986, **106**, pp 119-143.

https://doi.org/10.1017/S0001924000009969 Published online by Cambridge University Press

102. PHANINDRA, B.C. and RATHAKRISHNAN, E. Corrugated tabs for supersonic jet control, *AIAA J*, 2010, **48**, (2), pp 453-465.
103. ARUN KUMAR P. and RATHAKRISHNAN, E. Corrugated triangular tabs for supersonic jet control, Proceedings of the Institution of Mechanical Engineers, *Part G: J Aerospace Engineering*, 2014, **228**, (6), pp 831-845
104. ARUN KUMAR P. and RATHAKRISHNAN, E. Corrugated truncated triangular tabs for supersonic jet control, *J Fluids Engineering*, 2013, **135**, (9), 091104-11.
105. CLEMENT, S. and RATHAKRISHNAN, E. Characteristics of sonic jets with tabs, *Shock Waves*, 2006, **15**, pp 219-227.
106. IBRAHIM, M.K. and NAKAMURA, Y. Effects of rotating tabs on flow and acoustic fields of supersonic jet, *AIAA J*, 2001, **39**, pp 745-748.
107. HUSSAIN A.K.M.F. and HUSAIN H.S. Controlled excitation of elliptic jets, *Physics of Fluids*, 1983, **26**, pp 2763-2766.
108. HUSAIN, H.S. and HUSSAIN, A.K.M.F. Elliptic jets Part I: Characteristics of unexcited and excited jets, *J Fluid Mechanics*, 1989, **208**, pp 257-319.